Published in final edited form as:

Nat Neurosci. 2019 December ; 22(12): 2000–2012. doi:10.1038/s41593-019-0528-7.

Dynamic remodeling of a basolateral to central amygdala glutamatergic circuit across fear states

Nolan D. Hartley[1,4], **Andrew D. Gaulden**[1], **Rita Báldi**[1], **Nathan D. Winters**[1,4], **Gregory J. Salimando**[2,4], **Luis Eduardo Rosas-Vidal**[1], **Alexis Jameson**[1,4], **Danny G. Winder**[1,2,3,4], **Sachin Patel**[1,2,3,4,*]

[1]Department of Psychiatry and Behavioral Sciences, Vanderbilt University Medical Center, Nashville TN USA

[2]Department of Molecular Physiology & Biophysics, Vanderbilt University School of Medicine, Nashville TN USA

[3]Department of Pharmacology, Vanderbilt University School of Medicine, Nashville TN USA

[4]Vanderbilt Brain Institute, Vanderbilt University, Nashville TN USA

Abstract

Acquisition and extinction of learned fear responses utilize conserved but flexible neural circuits. Here we show that acquisition of conditioned freezing behavior is associated with dynamic remodeling of relative excitatory drive from the basolateral amygdala (BLA) away from corticotropin releasing factor-expressing (CRF+) central lateral amygdala (CeL) neurons, and toward non-CRF+ (CRF−) and somatostatin-expressing (SOM+) neurons, while fear extinction training remodels this circuit back toward favoring CRF+ neurons. Importantly, BLA activity is required for this experience-dependent remodeling, while directed inhibition of the BLA-CeL circuit impairs both fear memory acquisition and extinction memory retrieval. Additionally, ectopic excitation of CRF+ neurons impairs memory acquisition and facilities extinction, whereas CRF+ neuron inhibition impairs extinction memory retrieval, supporting the notion that CRF+ neurons serve to inhibit learned freezing behavior. These data suggest afferent-specific dynamic

*Correspondence to: Sachin Patel MD, PhD
, Professor of Psychiatry and Behavioral Sciences, Molecular Physiology & Biophysics, and Pharmacology, Vanderbilt University Medical Center, sachin.patel@vanderbilt.edu, 1601 23rd Avenue South, Nashville, TN 37232.

AUTHOR CONTRIBUTIONS

N.D.H. completed all experiments with assistance from A.D.G., R.B., N.D.W., L.E.R.V., and A.J. in the laboratory of S.P. G.J.S. completed RNA scope studies in the laboratory of D.G.W. N.D.H and S.P. conceived of and designed the studies and wrote the manuscript with input from all co-authors.

COMPETING INTERESTS

All authors declare no competing interests, however S.P. has received research contract support from H. Lundbeck A/S unrelated to the current work. S.P is also a scientific consultant for Psy therapeutics, Sophren Therapeutics, and H. Lundbeck A/S unrelated to the present work.

REPORTING SUMMARY

Further information on research design is available in the Nature Research Reporting Summary linked to this article.

DATA AVAILABILITY

The data sets generated during and/or analyzed during the current study are available from the corresponding author upon reasonable request.

remodeling of relative excitatory drive to functionally distinct subcortical neuronal-output populations represent an important mechanism underlying experience-dependent modification of behavioral selection.

INTRODUCTION

The CeA is a nodal structure at the limbic-motor interface critical for rapid action selection in response to changing environmental and homeostatic needs. Functionally distinct CeA neuron subpopulations have been found to coordinate conserved survival-oriented behaviors including freezing, flight, feeding, foraging, and hunting in mice[1-5]. Importantly, these diverse CeA-mediated behavioral responses can be guided by previous experience to ensure optimal behavioral selection during future environmental challenges[6]. One example of experience-dependent learning that has been extensively shown to recruit CeA neurocircuitry is Pavlovian fear conditioning, in which animals can form lasting associative memories between conditioned stimuli (CSs) and temporally coinciding aversive unconditioned stimuli (US)[7]. Importantly, these conditioned stimuli are reinforced during learning to serve as strong predictors of threat and are adaptive in the short-term. However, the proper extinction of fear responses to CSs when they no longer predict threat is an adaptive learning process as well, and is imperative for the normalization of behavior following traumatic stress exposure.

The CeA, containing almost entirely GABAergic medium-spiny like neurons, was previously thought to function as a passive output relay of conditioned stimulus information that would drive rapid and evolutionarily conserved fear responses, such as freezing behavior[8]. However, recent studies have provided evidence for the CeL as an essential regulator of fear memory formation and storage[1,9], suggesting it may also serve as an important nexus of synaptic plasticity for competing circuits that either promote the acquisition of conditioned fear responses or serve to suppress conditioned fear expression. Indeed, genetically or functionally distinguishable CeL neurons have been shown to have corresponding increases or decreases in activity to fear-promoting CSs[10,11], or extinction training, respectively[12], most commonly referred to as ‘CeL on’ and ‘CeL off’ neurons[8]. However, a mechanistic understanding of how excitatory afferent signals are capable of selecting distinct CeL cell types to drive the expression and extinction of fear responses is lacking.

CeA neurons that express the neuropeptide CRF have recently emerged as key determinants of both passive and active forms of fear expression in response to threat-predictive cues[2,13-15], as well as appetitive behavior under non-threatening conditions[16], suggesting CeA-CRF neurons control diverse survival-related behaviors depending on an animal’s context and previous experience. Here, we examined top-down and bottom-up excitatory afferents to CeL-CRF+ neurons following bipartite experiential learning and reveal how plasticity in the BLA-CeL circuit preferentially selects distinct neurons via changes in relative excitatory input strength between neighboring CRF+ and CRF− or SOM+ neurons. Our work also highlights an unexpected role for CeA CRF+ neurons in the regulation of fear extinction. Whereas CRF peptide release has been implicated in positively regulating fear

and anxiety behaviors[15,17], we find that CRF+ neuron activity also serves to reduce conditioned freezing responses.

RESULTS

Distribution, membrane properties and molecular phenotype of CeA CRF+ neurons.

Using a *CRF-IRES-Cre::Ai14* mouse reporter line, we found that CRF+ neurons are largely localized to the CeL (Fig. 1a,b), the primary input nucleus of the CeA[8]. CRF+ neurons in the CeL consist primarily of late firing neurons (Fig. 1c) and exhibit slight differences in basal membrane properties compared to CRF− neurons (Extended Data Fig. 1). CRF+ neurons have been described as being largely segregated from other genetically defined populations of neurons in the CeA[2,13]. Consistent with these previous studies, we find that CRF+ neurons in the CeL have minimal overlap with neurons expressing protein kinase Cδ (PKCδ+)[11,16,18,19]. We also find that CRF+ neurons demonstrate a detectable but low level of overlap with the neuropeptide marker SOM (Extended Data Fig. 1), which labels neurons necessary for the acquisition and expression of conditioned freezing[1,2,9]. Overlap with SOM + neurons was assessed using two methods, *in situ* hybridization and dual reporter mice, yielding different quantities of co-labeled neurons but consistent results in terms of the distribution of overlapping cells within the CeL (Extended Data Fig. 1). These data indicate that CRF+ neurons overlap only to a small degree with SOM+ neurons suggesting CRF+ neurons may regulate conditioned fear in ways unique to that of SOM+ and PKCδ+ neurons.

Fear conditioning and extinction training bidirectionally remodel relative glutamatergic input strength onto CeL CRF+ and CRF− neurons.

To begin to elucidate experience-dependent plasticity at excitatory glutamatergic inputs to the CeL, we performed *ex vivo* whole-cell patch-clamp recordings from naïve (basal), fear-conditioned, and fear-extinguished mice (Fig. 1d, and Supplementary Fig. 1). We alternated recordings of spontaneous excitatory post-synaptic currents (sEPSCs) from samples of closely neighboring CRF+ and CRF− neurons within the same plane of coronal brain slices (Fig. 1d,e). Using this approach, we found that average sEPSC frequency, but not amplitude, was significantly greater onto CRF+ neurons than CRF− neurons in naïve mice (Fig. 1f). However, following fear conditioning, average sEPSC frequency was not significantly different between CRF+ and CRF− neurons (Fig. 1g), but following extinction training, the average sEPSC frequency was again significantly greater onto CRF+ neurons than CRF− neurons (Fig. 1h).

To assess the relative influence of excitatory neurotransmission onto genetically distinct neurons, we plotted the sEPSC frequency and amplitude ratios of neighboring cell-types, a method of analysis that is sensitive to differences in input bias onto anatomically adjacent neurons[20]. We found that the CRF+/CRF− sEPSC frequency ratio was high in naïve mice, but significantly lower and close to 1:1 in fear-conditioned animals, and then was significantly higher again in mice that underwent extinction training (Fig. 1i). Analysis of average sEPSC frequency and amplitude for each cell-type across fear states revealed a shift in input bias away from CRF+ neurons that was driven by increased glutamatergic drive to CRF− cells (Fig. 1j), while the shift in relative input bias back onto CRF+ neurons following

extinction training was driven in part by an enhancement of excitatory neurotransmission onto CRF+ neurons as well as a concomitant reduction in excitatory neurotransmission onto CRF− neurons (Fig. 1j). These changes across fear states were reflected in sEPSC frequency, but not amplitude, suggesting a presynaptic locus of plasticity that contributes to shifts in input bias following fear conditioning and extinction training. Cumulatively, these results demonstrate that excitatory drive is biased toward CRF+ neurons under basal conditions, that this bias disappears with the acquisition of conditioned freezing, and then reemerges after extinction training.

Since the acquisition of conditioned freezing behavior requires a presynaptic strengthening of excitatory input onto SOM+ neurons[1], we wanted to confirm whether the increase in the sEPSC frequency onto CRF− neurons following fear conditioning is also occurring onto SOM+ neurons. Using *SOM-IRES-Cre::Ai14* reporter mice, we found significantly greater average sEPSC frequency onto SOM+ neurons in the CeL following fear conditioning relative to naïve mice (Extended Data Fig. 2). Furthermore, we found that the average sEPSC frequency was significantly reduced following extinction training, while there were no significant changes in average sEPSC amplitude across conditions, suggesting a population of CRF− neurons in this study likely consists of SOM+ neurons (Extended Data Fig. 2).

Fear conditioning produces circuit-specific remodeling of relative input strength onto CeL CRF+ and CRF− neurons.

Although our sEPSC recordings demonstrate the presence of experience-dependent shifts in relative excitatory drive to CRF+ and CRF− neurons, they do not provide information regarding which specific afferent inputs may be remodeled during fear acquisition and extinction. We therefore utilized optogenetic projection-targeting approaches to determine which afferent circuits to the CeL may contribute to experience-dependent shifts in relative input strength onto CRF+ and CRF− neurons and the potential expression mechanisms underlying observed circuit-specific plasticity. We bilaterally injected *CRF-IRES-Cre::Ai14* mice with an adeno-associated virus that drives the expression of channel rhodopsin (AAV-CamKIIα-ChR2-eYFP) into three brain regions known to send prominent glutamatergic projections to the CeL, all of which are necessary for intact fear learning (Fig. 2a): the BLA, which is responsible for relaying polymodal sensory information to the CeL regarding the CS[8], the insular cortex (INS), which relays interospective and visceral information to the CeL[21,22], and the parabrachial nucleus (PBN), which is a hindbrain projection largely responsible for conveying nociceptive and affective pain signals associated with the US (foot-shock) to the CeL[5]. Whole-cell recordings from CRF+ neurons in the CeL revealed TTX-sensitive fast optically-evoked excitatory post-synaptic currents (oEPSCs) from each afferent input, consistent with action potential dependent monosynaptic responses (Supplementary Fig. 2)[23-25].

We next performed simultaneous dual whole-cell patch-clamp recordings from CRF+ and proximally adjacent CRF− neurons from naïve and fear-conditioned mice (Fig. 2a) and examined the relative input strength onto both populations (Supplementary Fig. 3). Using this technique, we first sought to determine which afferent inputs could be regulating the

overall change in relative glutamatergic neurotransmission onto CRF+ and CRF− neurons following the acquisition of conditioned fear. Notably, the BLA-CeL circuit demonstrated an endogenous input bias characterized by greater relative input strength onto CRF+ neurons compared to CRF− neurons in naïve mice, which was quantified as a significant deviation from 1 in the slope of the linear regression of paired maximal oEPSC amplitude, and a high CRF+/CRF− maximal amplitude ratio (Fig. 2b-d). Importantly, this basal input bias was unaffected by exposure to the conditioning context or the CS+ in the absence of foot-shock (Extended Data Fig. 3). However, following fear conditioning, this input bias shifted away from CRF+ neurons, resulting in equal relative input strength onto CRF+ and CRF− neurons (Fig. 2b-d). In contrast to the BLA-CeL circuit, we found that the INS and PBN afferents to the CeL demonstrate a lack of input bias in naïve mice but following fear conditioning demonstrate a shift toward significantly greater relative input strength onto CRF+ neurons (Fig. 2e-l). Interestingly, traumatic stress exposure in the form of over-conditioning reproduced a similar pattern of changes in relative input strength in each of these circuitries as single-day conditioning, supporting the reliability of these observations (Supplementary Fig. 4). Cumulatively, these results indicate that each afferent projection examined dynamically remodels the weight of its synaptic input onto CRF+ and CRF− neurons following fear conditioning, but that plasticity within the BLA-CeL circuit is most closely associated with the overall changes in relative excitatory input onto CRF+ and CRF− neurons observed via measurement of sEPSCs (see Fig. 1).

The BLA-CeL circuit bidirectionally remodels following fear conditioning and extinction training.

Given that the BLA-CeL circuit most closely reflected the net changes in excitatory input bias seen in afferent-indiscriminate neurotransmission following fear conditioning (see Fig. 1), we next tested whether the BLA-CeL bias away from CRF+ neurons observed after conditioning normalizes following fear extinction. Fear-conditioned littermate mice were separated into two groups, one group that remained in their home cage for two days, and one group that received two days of extinction training (Fig. 3b), allowing a comparison between time-matched control and experimental groups while simultaneously testing for a persistence of synaptic changes and fear expression following fear memory formation. Importantly, mice that did not undergo extinction training showed elevated freezing behavior to the CS (Supplementary Fig. 1), marking a persistent retention of fear memory. In naïve mice, maximal oEPSC amplitudes from the BLA again showed a significant deviation from a linear regression of 1, indicating a bias in input strength favoring CRF+ neurons (Fig. 3c, d). As shown above, this bias disappeared following fear conditioning but reemerged after extinction training (Fig. 3d), an effect that was mirrored by changes in the CRF+/CRF− oEPSC amplitude ratios (Fig. 3e). These data suggest that the BLA-CeL circuit is bidirectionally remodeled by the acquisition and extinction of conditioned fear to alter relative input strength onto CRF+ and CRF− neurons across fear states.

Next, we sought to determine whether the BLA-CeL circuit contributes to the presynaptically-mediated alterations in input bias onto CRF+ and CRF− neurons. Since our sEPSC analysis only provides information regarding the net excitation from various inputs, individual input changes may go unnoticed due to counterbalancing or opposing plasticity at

other afferents. Therefore, to gain further mechanistic insight as to how the balance of excitatory input strength onto CRF+ and CRF− neurons is remodeled by fear acquisition and extinction, we examined BLA-CeL synapses via analysis of strontium-induced asynchronous EPSCs (aEPSCs) using *ex vivo* optogenetics (Fig. 4a-d). The advantage of this method is that it allows for a concurrent assessment of presynaptic and postsynaptic changes within an optogenetically isolated circuit[20,26,27], where optically evoked aEPSC amplitude provides a direct estimate of postsynaptic efficacy, while aEPSC frequency indirectly estimates number of synaptic release sites or release probability[20,28,29]. Using this method, we alternated recordings from closely neighboring pairs of CRF+ and CRF− neurons in the CeL and found that optically evoked aEPSCs from BLA-CeL synapses mirrored the previous experience-dependent changes in input-bias we observed after analysis of maximally evoked oEPSC amplitudes (Fig. 4e-i). Specifically, the CRF+/CRF− aEPSC frequency and amplitude measures were biased towards CRF+ neurons in the naive and fear-extinguished states, relative to the fear-conditioned state (Fig. 4f-i), suggesting the occurrence of both presynaptic and postsynaptic alterations in the BLA-CeL circuit contributing to the bidirectional change in input bias across fear states.

Since changes in aEPSC frequency can reflect either alterations in the number of synapses or neurotransmitter release probability, we differentiated between these two possibilities by alternating recordings from neighboring CRF+ and CRF− neurons and independently measuring the paired-pulse ratio (PPR) of BLA-CeL synapses, a measure that is inversely proportional to release probability (Extended Data Fig. 4). Although previous studies have noted changes in presynaptic release from the lateral amygdala (LA) to other neuronal populations in the CeL following fear conditioning[1,9], we did not find substantial differences in PPR of BLA-CeL synapses between CRF+ and CRF− neurons following fear conditioning or fear extinction (Extended Data Fig. 4), implying that the bidirectional changes in CRF+/CRF− aEPSC frequency ratios in this paradigm are more likely due to activity-driven adjustments in number of synaptic release sites onto these neurons. However, similarly to our observed changes in aEPSC amplitude ratios across fear states, examination of α-amino-3-hydroxy-5-methyl-4-isoxazoleproprionate receptor (AMPAR)/N-methyl-D-aspartate receptor (NMDAR) ratios further corroborated that post-synaptic modifications also contribute to shifts in relative input bias within the BLA-CeL CRF+/CRF− circuit (Extended Data Fig. 4). Overall, these studies provide converging evidence that the BLA-CeL circuit bidirectionally and dynamically changes its relative connectivity with CRF+ and CRF− neurons based on the animals' experience, with the naïve and fear-extinguished states associated with greater relative input strength onto CRF+ neurons, compared to the fear-conditioned state.

Given that fear conditioning enhances excitatory transmission onto CeL SOM+ neurons[1], we next sought to test whether the bidirectional shifts in relative input strength in the BLA-CeL circuit are reflected between populations of CRF+ and SOM+ neurons. To explicitly test this, we crossed CRF-IRES-Cre mice with SOM-IRES-Flp mice to gain genetic access to these distinct neuronal populations within the same animals, and co-injected Cre-dependent mCherry (AAV-hSyn-DIO-mCherry) and Flp-dependent YFP (AAV-EF1a-fDIO-YFP) into the CeA to label CRF+ and SOM+ neurons, respectively (Extended Data Fig. 1). The overall quantity of neurons co-expressing mCherry and YFP was low, with an average of 0.125, 1,

and 2 neurons co-labeled in the rostral, middle, and caudal CeL respectively (Extended Data Fig. 1). We then used the same labeling approach along with injection of ChR2-eYFP into the BLA, and performed dual whole-cell patch-clamp recordings from identified CRF+ and SOM+ neurons while stimulating the BLA-CeL circuit. Using this technique, we discovered the same bidirectional changes in input bias as we did for CRF+ and CRF− neurons, again suggesting that many of the CRF− neurons recorded in our previous analysis are likely SOM + cells (Extended Data Fig. 5). However, despite the total number of cells co-expressing these peptides being low, the possibility remains that inadvertent inclusion of CRF+/SOM+ neurons could affect the interpretability of electrophysiological results. We therefore determined changes in input bias in the BLA-CeL circuit between CRF+/SOM+ and CRF −/SOM− synapses. Interestingly, we found that CRF+/SOM+ and CRF−/SOM− neuron pairs showed input bias and ratiometric changes following fear conditioning and extinction training that is most consistent with that of CRF+ and CRF− pairs (Supplementary Fig. 5). Thus, our data suggests that neurons expressing both CRF and SOM are more similar to neurons that only express CRF, at least in terms of their circuit-specific experience-dependent plasticity.

BLA-CeL circuit remodeling onto CRF+ and CRF− neurons is activity-dependent.

We next examined whether activity of the BLA is necessary for fear-conditioning-induced synaptic remodeling of BLA-CeL synapses onto CRF+/CRF− neurons. To test this, we used a chemogenetic method involving the use of designer receptors exclusively activated by designer drugs (DREADDs)[30]. *CRF-IRES-Cre::Ai14* mice were bilaterally co-injected into the BLA with AAV-CamKIIα-ChR2-eYFP and the inhibitory Gαi-coupled DREADD (AAV-CamKIIα-hM4Di-mCherry), and subsequently administered VEH or clozapine-*N*-oxide (CNO) prior to conditioning (Fig. 5a-c). Importantly, bath application of CNO in these mice depressed oEPSC amplitude from the BLA projection onto CeL neurons, suggesting this approach can inhibit neurotransmitter release and decrease the signaling fidelity of the BLA-CeL circuit (Fig. 5b). Consistent with our previous experiments, dual patch-clamp recordings yielded the same basal input bias from the BLA-CeL circuit onto CRF+ neurons and a high CRF+/CRF− amplitude ratio, which disappeared following fear-conditioning in VEH-treated mice (Fig. 5d-f). However, these changes in input strength following fear-conditioning were absent in CNO-treated animals (Fig. 5d-f), indicating that activity within principal BLA neurons during fear conditioning is necessary for driving the relative shifts in BLA-CeL input strength away from CRF+ neurons. Similarly, we administered VEH or CNO prior to extinction training in a separate cohort of mice (Fig. 5g). We found that inhibiting the BLA prior to both days of extinction training blocked the shift in input bias back towards CRF+ neurons (Fig. 5h-j). Overall, these findings demonstrate that BLA activity is necessary for the bidirectional shifts in input bias onto CRF+ and CRF− neurons that occurs with the acquisition and extinction of conditioned fear. Importantly, mice given CNO that expressed mCherry instead of the Gαi-coupled DREADD in the BLA did not demonstrate differences in input bias from VEH treated mice, indicating CNO alone does not affect BLA-CeL circuit remodeling (Supplementary Fig. 6).

The BLA-CeL circuit is necessary for fear memory acquisition and the retrieval of extinction memory.

Because the BLA-CeL circuit remodels input to CeL neurons across fear states in an activity-dependent manner, we next tested the potential relevance of this circuit remodeling to the acquisition and extinction of conditioned fear. Whole BLA inhibition has been shown to differentially affect fear behavior compared to directed manipulations of distinct BLA projection neurons[31-33]. Therefore, to selectively inhibit the BLA-CeL circuit, we used an intersectional genetic strategy in which we bilaterally injected the CeA with a retrograde virus that drives the expression of the cre-recombinase enzyme (AAVrg-Cre)[34], and in the same mice bilaterally injected the BLA with a virus that drives the expression of the inhibitory Gαi-coupled DREADD in a cre-dependent manner (AAV-hSyn-DIO-hM4Di-mCherry) (Fig. 6a). Mice injected with CNO prior to conditioning had significantly diminished freezing relative to VEH-treated mice in response to CS presentation the following day (Fig. 6b,c), indicating that the activity of BLA-CeL projection neurons critically contributes to the acquisition of fear memories as assessed by memory recall the following day, without affecting freezing during conditioning *per se*. In separate mice injected with CNO prior to extinction training sessions, we did not find differences in within-session conditioned freezing responses or freezing responses during an extinction memory recall test the following day (Fig. 6d,e), suggesting that the activity of the BLA-CeL circuit is not necessary for the acquisition of extinction memory. However, since BLA afferents dynamically normalize input bias to the CeL after extinction training, it is possible that activity of this circuit may serve to decrease conditioned freezing responses after synaptic remodeling has already occurred. Consistent with this possibility, we found that decreasing the excitability of the BLA-CeL circuit with CNO during an extinction memory recall test, at a time point in which the circuit input bias has shifted back towards favoring CRF+ neurons, caused a significantly greater level of freezing compared to VEH-treated controls, suggesting the BLA-CeL circuit is also necessary for the optimal retrieval of extinction memory (Fig. 6 f,g).

CRF+ neuron activity is sufficient to impair fear memory acquisition and facilitate within session extinction, and is necessary for extinction memory retrieval.

CeA CRF+ neurons have been shown to form mutually inhibitory synapses with SOM+ neurons, a circuit motif that may allow for rapid selection of divergent threat-adaptive responses via a mechanism of competitive lateral inhibition[2]. Given our data demonstrating that CRF+ neurons receive greater relative BLA excitatory input under basal and fear-extinguished conditions than CRF−/SOM+ neurons, and SOM+ neurons drive freezing responses[1,2,9], it is possible that CRF+ neuronal activity may serve to reduce freezing behavior. To test this idea, and probe the functional role of CeA-CRF+ neurons in regulating passive fear behavior, CRF-IRES-Cre mice were bilaterally injected into the CeA with a cre-dependent excitatory Gαq-coupled DREADD (AAV-hSyn-DIO-hM3Dq-mCherry, Fig. 7a) to increase the excitability of CRF+ neurons. Importantly, we found that bath application of CNO produced a significant depolarization of the resting membrane potential (Fig. 7b), and that systemic injection of CNO increased the expression of the immediate early gene Fos in mCherry+ neurons, validating this methodological approach (Extended Data Fig. 6).

Next, we increased the excitability of CRF+ neurons *in vivo* by injecting CNO or VEH prior to fear conditioning, at a time point when the relative input bias of the CeL network favors CRF+ neurons, but when a shift in relative input away from CRF+ neurons would be expected to be initiated (Fig. 7c,d). Animals injected with CNO had lower freezing to the CS than VEH-treated animals during fear memory recall the following day, without differences in within-session freezing during conditioning, suggesting impaired fear memory acquisition (Fig. 7e). Moreover, increasing the excitability of CRF+ neurons during extinction training, at a time point when relative input bias has already shifted away from CRF+ neurons towards equal input onto CRF+ and CRF−/SOM+ neurons, caused a significant reduction in within-session freezing behavior (Fig. 7f,g). However, enhancement of CRF+ neuron activity did not affect the initial retrieval of fear memory (freezing during the first 2 CS presentations on d2), suggesting that activity of CRF+ neurons promotes within-session extinction rather than simply gating the expression of freezing responses. Additionally, enhancing the excitability of CRF+ neurons did not affect the speed of the same mice when they were presented with the CS, or cause signatures of CRF-mediated plasticity within the CeL, indicating that activity of CRF+ neurons does not induce escape or flight-like responses in this paradigm, and that our rapid behavioral effects are not likely due to local CRF release within the CeL (Extended Data Fig. 6). Overall, these data reveal that CeA-CRF+ neuron activity is sufficient to diminish passive fear expression, an effect consistent with the relatively greater excitatory input from the BLA onto these cells in low fear states.

We further addressed the necessity of CRF+ neurons for the extinction of conditioned freezing by bilaterally expressing a cre-dependent inhibitory Gαi-coupled DREADD (AAV-hSyn-DIO-hM4Di-mCherry) in the CeA of our CRF-IRES-Cre mice (Fig. 7h). As expected, we found that bath application of CNO produced a significant hyperpolarization of the resting membrane potential, resulting in the complete blockade of action potential firing in CRF+ neurons (Fig. 7i). We then injected CNO or VEH prior to extinction training sessions and found that decreasing the excitability of CRF+ neurons, at a time-point where the relative excitatory input bias onto CRF+ and CRF− neurons is equal, did not prevent within-session extinction or extinction memory recall (Fig. 7j,k). However, our whole-cell recordings indicate that relative excitatory input bias shifts back onto CRF+ neurons following two days of extinction training (i.e. day 4, Fig. 7c), suggesting that CRF+ neuron activity may be important for the subsequent retrieval, rather than acquisition, of extinction memory *per se*. To test this hypothesis, we injected a separate cohort of mice with CNO or VEH prior to an extinction memory recall session (Fig. 7l). Consistent with this hypothesis, decreasing CRF+ neuronal activity at a time point at which CRF+ neurons receive greater excitatory input caused a significantly greater level of freezing relative to VEH treatment (Fig. 7l,m), revealing the necessity of CeL CRF+ neurons for full extinction memory retrieval. Importantly, CNO administration in wild-type or mCherry-only expressing mice at each of the time points examined for DREADD manipulations did not affect freezing levels, indicating our results were not due to off-target actions of CNO (Supplementary Fig. 7).[35]

Cumulatively, our findings and those of previous studies suggest CRF+ and SOM+ neurons are important for passive fear inhibition and expression, respectively[1,36,37]. Given the functional differences in these cell-types, we next explored differences in the output circuitry of these neurons, which could inform upon their divergent behavioral roles. Whole-brain

optogenetic output mapping revealed a large number of convergent brain structures between these classes of CeA neurons, as well as a number of divergent brain structures in which CRF+ and SOM+ neurons differentially project (Supplementary Fig. 8,9). Considering the periaqueductal gray (PAG) and the CeA are brain regions that are indispensable for the expression of defensive fear behaviors[38,39], we examined the degrees of connectivity within sub-regions of these nuclei from CRF+ and SOM+ neurons. Notably, whole-cell recordings in the CeL and PAG demonstrated optically evoked inhibitory postsynaptic currents (oIPSCs) that were blocked by application of the $GABA_A$ receptor antagonist picrotoxin, consistent with both local and long-range projections of SOM+ and CRF+ neurons signaling through GABAergic neurotransmission (Extended Data Fig. 7). Furthermore, SOM+ efferent projections terminate in the ventral/ventrolateral PAG (v/vlPAG) with a smaller degree of terminals also present in the dorsal/dorsolateral PAG (d/dlPAG), whereas CRF+ efferent projections primarily terminate in the v/vlPAG (Supplementary Fig. 8,10). These results indicate that each neuronal population may differentially affect motor output from the PAG in cooperation with signals from other upstream brain structures. A similar connectivity pattern was seen for CRF+ neuronal output to brain regions with high or low terminal expression (Supplementary Fig. 10).

DISCUSSION

The acquisition of conditioned fear responses is essential to survival, allowing organisms to properly assess and avoid harm when re-exposed to threat-predictive stimuli in the environment. Conversely, learning to suppress and diminish conditioned fear responses when a CS no longer signals immediate danger is also essential. Indeed, impairments in extinction learning are a phenotypic hallmark of posttraumatic stress disorder[40]. Here we show that acquisition of conditioned fear memories is associated with an activity-dependent shift in BLA glutamatergic input bias away from CRF+ CeL neurons and toward CRF −/SOM+ neurons, while extinction training is associated with a reversal of input bias. Our data suggest these shifts in input bias are likely mediated by both postsynaptic modifications and possibly changes in presynaptic contacts. We also found that reducing neuronal activity within the BLA during conditioning prevents the relative shift in input bias away from CRF+ cells, while specifically decreasing signaling of the BLA-CeL circuit reduces fear memory acquisition as assessed by next-day recall. Although our plasticity experiments were restricted to global manipulations of BLA neurons, these data provide indirect but converging evidence that activity-dependent remodeling of the BLA-CeL circuit may be a physiological correlate for optimal fear memory acquisition. Additionally, previous work has demonstrated that inhibition of the BLA-CeM circuit reduces within-session freezing during conditioning but not fear memory recall the following day[33], suggesting that BLA neurons that project distinctly to the CeM and CeL may play separate but complimentary roles in driving freezing responses during initial threat exposure versus the future behavioral selection of these responses following associative learning, respectively. In contrast, inhibition of the BLA-CeL circuit during extinction training in our studies did not impair within-session extinction learning or extinction memory recall, although reductions in BLA activity during extinction training did prevent extinction-induced synaptic remodeling. Together, these results suggest that compensatory circuits are still able to support fear

extinction in the face of compromised BLA-CeL remodeling. However, inhibition of the BLA-CeL circuit, or inhibition of CRF+ neurons downstream of the BLA, did impair extinction memory retrieval, suggesting compensatory circuits cannot override a reduction in the activity of this circuit after proper remodeling has already taken place. These findings provide new insight into how BLA afferents to distinct CeL neuronal populations remodel across fear states, and the relationship between these synaptic adaptations and fear or extinction learning.

A key finding of the present work is that CeL CRF− neurons receive enhanced excitatory drive after fear conditioning. It is likely at least a subpopulation of CRF− neurons in this study are SOM+ neurons, which have been shown to be essential in producing conditioned and unconditioned freezing behavior[1,2,9]. Consistent with this possibility, we found bidirectional enhancement and reduction of excitatory neurotransmission onto SOM+ neurons following fear conditioning and extinction training that closely mirrored that of CRF− neurons. That ectopic activation of CeA CRF+ neurons reduces conditioned freezing further supports the notion CRF+ and SOM+ neurons generate antagonistic behavioral responses to threat-predictive cues[2,41]. Given that both CRF+ and SOM+ neurons are GABAergic, differences in connectivity and signaling to converging brain structures or distinct projections to diverging brain structures may represent a neural substrate for the antagonistic effects of these neurons on freezing behavior, and require further investigation.

Temporally precise control of CRF+ neuronal activity using *in vivo* optogenetics has shown that CRF+ neurons drive active motor responses including escape and conditioned flight behavior to CS presentation, which are associated with strong inhibitory control over SOM+ neurons[2]. Therefore, it appears CRF+ neurons may use fast GABAergic neurotransmission and lateral inhibition of SOM+ neurons to trigger active phenotypes, whereas CRF peptide release from these cells has been implicated in generating passive freezing responses via the enhancement of synaptic neurotransmission onto CRF1 receptor-expressing neurons in the CeA (of which a large proportion are SOM+; Supplementary Fig. 11)[13]. In line with this idea, neuropeptides are often only released from dense core vesicles following bouts of prolonged neural activity or high firing rates and signal through G-protein coupled receptors, which generally have a slower influence on membrane excitability than fast neurotransmission[42]. As a parallel to this concept, SOM signaling in the amygdala has been shown to decrease anxiety and fear expression[43-45], suggesting SOM+ neurons may utilize fast neurotransmission to drive freezing responses, but SOM release may serve as a homeostatic feedback mechanism for preventing fear generalization and maladaptive fear expression over time. Future studies should aim at investigating the interplay and differences between the use of fast neurotransmission and neuropeptide signaling within genetically defined cell populations in the CeL.

Our findings also emphasize that the balance of relative BLA input to distinct CeL cell-types may be more informative for assessing experience-dependent learning within this system than changes in the absolute input-magnitude onto a single cell-type. In this context, it has been previously suggested that the BLA is responsible for switching between states of high and low fear expression and that separate BLA “fear-on” and “fear-off” neurons contribute to fear expression and extinction, respectively[46,47]. These findings raise the possibility that

changes in relative excitatory drive to CRF+ and CRF−/SOM+ neurons after fear conditioning and extinction training could be driven by inputs from distinct BLA cell populations. Future studies will be required to experimentally test this hypothesis.

In light of the diverse behavioral responses CRF+ neurons can influence, we propose a model in which these neurons regulate an animal's motor output by promoting active motivational responses. In naive mice, activity of these neurons would stimulate promotor output to influence the expression of active responses associated with appetitive drive[16], such as surveying the environment for resources, foraging, or approach responses (Supplementary Fig. 11). Alternatively, under conditions of imminent threat activity of these neurons can initiate active promotor behaviors such as escape or flight-like responses[2,39], whereas under conditions of safety or subsiding fear, the activity of CRF+ neurons will promote active exploration[16]. Thus, as the contingency between the CS and US degrades during extinction training, greater relative input is restored back onto CRF+ neurons to diminish passive freezing responses and facilitate active exploration of the environment (Supplementary Fig. 11).

During exposure to a threat, an animal's survival depends on rapidly assessing environmental cues and mounting optimal behavioral responses including freezing, escape, or avoidance. Conversely, under non-threatening conditions, survival depends on the ability to explore and pursue meaningful stimuli in the environment. In any given environmental context, multiple brain circuits coordinate through parallel processes to determine the ultimate behavioral strategies an animal selects. Our findings support an emerging view that experience-dependent plasticity mechanisms that shift the balance of top-down excitatory drive to distinct classes of sub-cortical neurons may represent a conserved mechanism for optimizing behavioral action selection in response to previous experiences[20].

METHODS

Animals.

All experiments were approved by the Vanderbilt University Institutional Animal Care and Use Committees and were conducted in accordance with the National Institute of Health Guide for the Care and Use of Laboratory Animals. Male 7-15 week old wild type, CRF-IRES-Cre (Jackson Laboratory strain B6(Cg)-Crhtm1(cre)Zjh/J; stock #: 012704; donating investigator Z. Josh Huang, Cold Spring Harbor Laboratory), CRF-IRES-Cre::Ai14 (CRF-IRES-Cre crossed to Jackson Laboratory strain B6.Cg-Gt(ROSA)26Sortm14(CAG-tdTomato)Hze/J; stock #: 007914; donating investigator Hongkui Zeng, Allen Institute for Brain Science), SOM-IRES-Cre (Jackson Laboratory strain B6J.Cg-Ssttm2.1(cre)Zjh/MwarJ; stock #: 028864; donating investigator Z. Josh Huang, Cold Spring Harbor Laboratory & Melissa R Warden, Cornell University), SOM-IRES-Cre::Ai14, CRF-IRES-Cre::SOM-IRES-Flp (CRF-IRES-Cre crossed to Jackson Laboratory strain Ssttm3.1(flpo)Zjh/J; stock #028579; donating investigator Z. Josh Huang, Cold Spring Harbor Laboratory) mice on a C57/BL6J background, or a mixed C57/BL6J/?+pN1F9 background for CRF-IRES-Cre::SOM-IRES-Flp mice were used for all experiments where indicated in the text. Mice were housed no more than 5 animals per cage in a temperature and humidity-controlled housing facility under a 12h light/dark cycle with ad libitum access

to food and water. For electrophysiology recordings from naïve, fear, or extinction groups, mice were single housed following behavioral manipulation to avoid naïve mice being exposed to stressed littermates. All experiments were performed during the light cycle.

Viruses.

For ex vivo circuit mapping of inputs and outputs to the CeL, we used AAV5-CaMKIIα-ChR2(H134R)-eYFP (0.15-0.25μL) and AAV5-EF1α-DIO-ChR2(H134R)-eYFP (0.3μL), respectively (UPenn Vector Core, Philadelphia, PA, or Addgene, Watertown, MA). For chemogenetic manipulations in the CeA we used AAV5-hSyn-DIO-hM3D(Gq)-mCherry and AAV5-hSyn-DIO-hM4D(Gi)-mCherry (1μL). For bilateral co-injection of AAV5-CaMKIIα-hM4D(Gi)-mCherry and AAV5-CaMKIIα-ChR2(H134R)-eYFP or AAV5-hSyn-mCherry into the BLA (0.15μL), we combined viruses in a 1:1 ratio. For circuit specific DREADD approaches we bilaterally injected the retrograde specific AAV2rg-pmSyn1-eBFP-Cre variant (0.1μL) into the CeA and bilaterally injected the cre-dependent AAV5-hSyn-DIO-hM4D(Gi)-mCherry or AAV5-hSyn-DIO-mCherry (0.2μL) into the BLA. For fluorescent labeling of CRF+ and SOM+ neurons in CRF-IRES-Cre::SOM-IRES-Flp mice with bilateral targeting to the CeA (0.3μL), we combined AAV5-hSyn-DIO-mCherry and AAV5-EF1a-fDIO-eYFP in a 1:1 ratio. AAV2rg-pmSyn1-eBFP-Cre was a generous gift from Hongkui Zeng (Addgene viral prep # 51507-AAVrg)[48]). AAV5-hSyn-DIO-hM3D(Gq)-mCherry, AAV5-hSyn-DIO-hM4D(Gi)-mCherry, AAV5-CaMKIIα-hM4D(Gi)-mCherry, and AAV5-hSyn-DIO-mCherry were all generous gifts from Bryan Roth (Addgene viral preps # 44361-AAV5, # 44362-AAV5, and # 50477-AAV5)[49]. AAV5-CaMKIIα-ChR2(H134R)-eYFP, AAV5-EF1α-DIO-ChR2(H134R)-eYFP, AAV5-EF1a-fDIO-eYFP and AAV5-hSyn-mCherry were all generous gifts from Karl Deisseroth (UPenn Vector Core, Philadelphia, PA, and Addgene viral preps # 26969-AAV5, # 20298-AAV5, # 55641-AAV5, # 114472).

Surgery.

Mice were anesthetized with 5% isoflurane and then transferred to a stereotaxic frame (Kopf Instruments, Tujunga, CA) and kept under constant 2.5% isoflurane anesthesia. The skull surface was exposed via a midline sagittal incision and treated with the local anesthetic benzocaine (Medline Industries, Brentwood, TN). For each surgery, a 10uL microinjection syringe (Hamilton Co., Reno, NV) with a Micro4 pump controller (World Precision Instruments, Sarasota, FL) was guided by a motorized digital software (NeuroStar; Stoelting Co., Wood Dale, IL) to each injection coordinate. Virus was administered bilaterally into the CeA (coordinates in mm: AP: −0.70-1.15, ML: ±2.93, DV: 4.31-4.60 from Bregma), the BLA (coordinates in mm: AP: −1.25-1.50, ML: ±3.35-3.60, DV: 5.00 from Bregma), the INS (coordinates in mm: AP: −0.10, ML: ±4.10, DV: 4.30 from Bregma), and the PBN (coordinates in mm: AP: −4.75, ML: ±1.40, DV: 3.67 from bregma). Following completion of surgery, 10mg/kg ketoprofen (AlliVet, St. Hialeah, FL) was administered as an analgesic.

Immunohistochemistry and imaging.

Mice were anesthetized using isoflurane (Abbott Labs, Chicago, IL) and transcardially perfused with cold phosphate buffered saline (PBS, 10mL) followed by cold 4% paraformaldehyde in 0.1M phosphate buffer (PFA, 15-20mL). Brains were dissected and

stored overnight at 4o C in 4% PFA and then transferred to a 30% sucrose solution for 4 days, were cut at 40μm using a Leica CM3050 S cryostat (Leica Microsytems, Weitzlar, Germany), and subsequently placed in an ethylene-glycol-based antifreeze solution at −20o C for long-term storage. Brain slices were washed in Tris-Buffered Saline (TBS) for 3X 10min, placed in TBS with 4% Horse serum and 0.2% Triton X-100 (TBS+) for 30min, followed by overnight incubation with primary antibodies: mouse anti-PKCδ (1:500; BD Biosciences, San Jose, CA, 611463), rabbit anti-c-Fos (1:500; Millipore, Burlington, MA, ABE457), or chicken anti-GFP (1:500; Abcam, Cambridge, UK, ab13970). Slices were washed 3X 10min in TBS+ and incubated for 2.5hrs with secondary antibody: Alexa Fluor 488 donkey anti-rabbit or donkey anti-mouse (1:1000; Invitrogen, Carlsbad, CA, A21206), or Cy2 AffiniPure donkey anti-chicken (1:1000; Jackson ImmunoResearch Laboratories Inc., 703-225-155), washed for 3X 10min in TBS and then mounted and cover-slipped. For slices stained with 4′,6-diamidin-2-phenylindol (DAPI, 1:12,000; Thermo Fisher Scientific, Waltham, MA, 62248) we incubated for 5 min, followed by an extra 3X 10min washes in TBS. Imaging was conducted using an upright Axio Imager M2 epifluorescent microscope or a Zeiss inverted LSM 710 Meta confocal microscope (Zeiss, Oberkochen, Germany). Whole brain section images were acquired by tiling using a 5X objective, and higher magnification images were acquired by tiling the amygdala using a 20X objective. Brightness and contrast of images were adjusted using Image J or Adobe CS4 software for clarity and presentation in figures.

Cell counting and co-localization.

Fluorescently labeled neurons in the CeC, CeL, and CeM were counted using ImageJ software (Public Domain license, Wayne Rasband) between stereotaxic brain coordinates −1.06mm and −1.70mm from Bregma. Cell counts were analyzed along the rostrocaudal axis of the CeA by identifying a representative coronal slice from each animal for rostral (−1.06-1.22mm from bregma), middle (−1.34-1.46mm), and caudal (−1.58-1.70mm) subdivisions using whole-brain stereotaxic coordinates atlas as a reference (Franklin & Paxinos, 2007). Exposure was kept the same between groups when imaging C-fos positive neurons in the CeL, and adjustments for brightness or contrast were done equally in parallel between groups.

RNAscope® fluorescent *in situ* hybridization.

RNAscope® cDNA probes and detection kits were purchased from ACD and used according to the company's online protocol for fresh frozen tissue. The probe sets directed against CRF, SOM, and PKCδ were designed from sequence information from the mouse RefSeq mRNA IDs NM_205769.2, NM_009215.1, and NM_011103.3, respectively (more information available on ACD's website). Mice were anesthetized using isoflurane and the brains were quickly removed and frozen in Tissue Tek® O.C.T. compound (Sakura Finetek, Torrance, CA) using Super Friendly Freeze-It Spray (Fisher Scientific, Hampton, NH). Brains were stored at −20°C until cut on a cryostat to produce 16 um coronal sections. Sections were adhered to warm slides and immediately refrozen before being stored at −80°C until ready to undergo the RNAscope® procedure. Following the ACD protocol for fresh frozen tissue, slides were fixed for 15 mins in ice cold 4% paraformaldehyde and then dehydrated in a sequence of ethanol serial dilutions (50%, 70% and 100%, twice each).

Slides were briefly air-dried and then a hydrophobic barrier was drawn around the tissue sections using a Pap Pen (Vector Labs). Slides were then incubated with ACD's protease IV solution for 30 mins at room temperature in a humidified chamber. Following protease treatment, sections were incubated with RNAscope® cDNA probes (2 hours), and then with a series of signal amplification reagents provided by the Multiplex Fluorescence Kit from ACD; in brief, Amp 1-FL (30 mins), Amp 2-FL (15 mins), Amp 3-FL (30 mins) and Amp 4-FL ALT A (15 mins). Two minutes of washing in RNAscope® wash buffer (1x from 50x stock, ACD) were performed between each step, and all incubation steps with the cDNA probes and amplification reagents were preformed using a HybEZ oven (ACD) at 40°C. cDNA probe mixtures were prepared at a dilution of 50:1:1 for SOM, CRF and PKCδ, respectively. Sections were also stained for DAPI using the reagent provided by the Fluorescent Multiplex Kit. Immediately following DAPI staining, sections were mounted and cover slipped using Aqua-Polymount (PolySciences) and left to dry overnight. Slides from the anterior, medial and posterior CeA were collected in pairs, using one section for incubation with the cDNA probes, and another for incubation with a 3 probe set for bacterial mRNA (DapB; ACD) to serve as a negative control.

Sections were imaged using a Zeiss inverted LSM 710 Meta confocal microscope at 20X and 63X magnification. Images from sections treated with the negative control probe for each pair of slides were used to determine brightness and contrast parameters that minimized observation of bacterial transcripts and auto-fluorescence, and these adjustments were then applied to the images in parallel from experimental sections treated with the cDNA probes. Adjusted experimental images were then analyzed in a designated region of interest around the CeL. Cells in these regions of interest were identified using both the DAPI stained nuclei and the borders present between cells (identified with the help of gray scale differential interference contrast (DIC) overlays), and the total number of cells in each region were counted. Cells were then counted for presence of CRF, SOM, and PKCδ signal in order to determine totals for each cell population expressing these signals either alone or in various combinations. Transcripts were readily identified as round, fraction delimited spots over and surrounding DAPI-labeled nuclei.

Fear conditioning and extinction training.

Mice underwent fear conditioning and extinction training as previously described[50]. Briefly, mice were placed in Context A for fear conditioning, which consisted of a chamber with dimensions: 30.5 × 24.1 × 21.0cm and an automated freezing analysis software (Med Associates, Burlington, VT, USA), which was cleaned prior to and in between mice using MB-10 disinfectant (Quip Laboratories, Wilmington, DE). For conditioning (day 1), mice were presented with six conditioned stimulus- unconditioned stimulus (CS-US) pairings (tone-foot shock) separated by a 30s inter-trial interval (ITI). Each tone (80 dB, 3000 Hz) lasted 30s. Mice were presented with the electric foot shock at 0.7mA during the last 2s of each 30s tone. For fear extinction training, day 2 and day 3, mice were placed in Context B, which consisted of the same chamber with a white floor, a curved white wall contextual insert, and a distinct vanilla extract olfactory cue (McCormick, Sparks, MD). A short 30s baseline was used to test initial freezing as a measure of fear generalization to the novel context. Mice were then presented with 20 CS presentations (30s) with a 30s ITI. For

extinction recall (day 4), mice were placed back into Context B the following day and presented with 6 CS presentations with a 30s ITI. For some experiments, a full drug-free extinction session on day 2 or day 4 was conducted to compare early and late phase fear or extinction recall, and the first 5-6 CS presentations were used as a measure of recall in the absence of drug administration. Conditioned flight behavior was scored by measuring the speed of mice during extinction training using ANY-maze automated software (Stoelting, Wood Dale, IL).

Ex vivo electrophysiology.

Coronal brain sections were collected at 250μm using standard procedures. Mice were anesthetized using isoflurane, and transcardially perfused in an ice-cold/oxygenated (95% v/v O2, 5% v/v CO2) cutting solution consisting of (in mM): 93 N-Methyl-D-glucamine (NMDG), 2.5 KCl, 20 HEPES, 10 MgSO4. 7H2O, 1.2 NaH2PO4, 30 NaHCO3, 0.5 CaCl2. 2H2O, 25 glucose, 3 Na+-pyruvate, 5 Na+-ascorbate, and 5 N-acetylcysteine. The brain was subsequently dissected, hemisected, and sectioned using a vibrating LeicaVT1000S microtome (Leica Microsytems, Bannockburn, IL). The brain slices were then transferred to an oxygenated 34°C chamber filled with the same cutting solution for a 10 min recovery period. Slices were then transferred to a holding chamber containing a buffered solution consisting of (in mM): 92 NaCl, 2.5 KCl, 20 HEPES, 2 MgSO4 7H2O, 1.2 NaH2PO4, 30 NaHCO3, 2 CaCl2 2H2O, 25 glucose, 3 Na-pyruvate, 5 Na-ascorbate, 5 N-acetylcysteine and were allowed to recover for ≥30 min. For recording, slices were placed into a perfusion chamber where they were constantly exposed to oxygenated artificial cerebrospinal fluid (ACSF; 31-33°C) consisting of (in mM): 113 NaCl, 2.5 KCl, 1.2 MgSO4. 7H2O, 2.5 CaCl2. 2H2O, 1 NaH2PO4, 26 NaHCO3, 20 glucose, 3 Na+-pyruvate, 1 Na+-ascorbate, at a flow rate of 2-3ml/min.

Cells were visually identified from Ai14 reporter lines or virally injected animals under illumination from a series 120Q X-cite lamp at 40X magnification using an immersion objective in coordination with differential interference contrast microscopy (DIC). CeL neurons were voltage clamped in whole cell configuration at −70mV using borosilicate glass pipettes (3-6MΩ) filled with intracellular solution containing (in mM): 125 K+-gluconate, 4 NaCl, 10 HEPES, 4 MgATP, 0.3 Na-GTP, and 10 Na-phosphocreatine (pH 7.30-7.35). To assess basal membrane properties and sEPSCs onto distinct CeL cell types, alternating whole-cell patch clamp recordings were made from neighboring (≤30μm) TdTomato expressing somata (CRF+) or TdTomato lacking somata (CRF−) within the same depth and plane of the slice, or independently from SOM+ neurons in other animals as depicted in figures. Following break-in to each cell, ≥3 min of time elapsed before initiation of experiments to allow for internal solution exchange and stabilization of membrane properties. Spontaneous excitatory post-synaptic currents (sEPSCs) were recorded over 3 min in the presence of the $GABA_A$ receptor antagonist picrotoxin (25μM) so as to isolate excitatory neurotransmission. After sEPSC recordings, cells were switched to current clamp configuration, resting membrane potential was recorded, and then current injection was manually applied to maintain the cell near a stable resting potential of −70mV. Depolarizing current injections (20, 600ms) were administered in incremental steps (Δ40pA) beginning with an initial hyperpolarizing current injection of −100pA. The afterhyperpolarization

(AHP) amplitude was measured by applying 5 sweeps of a 600pA current injection (400ms). The time constant was determined using 5 sweeps of a −100pA current injection (10ms). Input resistance was measured using 10 sweeps of a −20pA current injection (500ms). When possible, all membrane properties were measured from each recorded neuron following sEPSC recordings. For recordings of PPR and AMPAR/NMDAR ratios we used an internal solution containing (in mM): 120 Cs-gluconate, 2.8 NaCl, 20 HEPES, 2.5 MgATP, 0.25 Na-GTP, and 5 TEA-Cl (pH 7.30-7.35). All data was acquired using a Multiclamp 700B amplifier, Digidata 1440A A/D converter, Clampex version 10.6 software (Axon Instruments, Union City, CA), was sampled at 20kHz and low pass filtered at 1 kHz, and analyzed in Multiclamp version 10.6 software (Axon Instruments).

Ex vivo optogenetics.

For input mapping experiments, mice were bilaterally injected with AAV5-CaMKIIα-ChR2(H134R)-eYFP into the BLA, INS, or PBN using cohorts of CRF-IRES-Cre::Ai14 mice. When possible, cohorts of littermate mice were equally distributed between experimental groups to limit inter-cohort variability. Mice recovered for 4 weeks to allow for maximal virus expression and then were randomly assigned to naïve (basal), fear, or extinction groups. For the majority of experiments, recordings from each group were interleaved daily when applicable. For comparisons between inputs onto CRF+ neurons, we performed input/output curves by incrementally stepping light exposure time while keeping light intensity constant (3.0 mW/mm^2). Dual whole-cell patch clamp recordings were conducted from neighboring CRF+ and CRF− neurons (somata ~ ≤30μm), CRF+ and SOM+ neurons (somata ~ ≤60μm), or CRF+/SOM+ and CRF−/SOM− neurons (somata ~ ≤30μm). Series resistance compensation (≤75%) was used to approximately match access resistance values between each cell (within 0-3MΩ). We recorded oEPSCs elicited from the BLA, INS, and PBN inputs by illuminating the central amygdala with ~470nm wavelength light using a LEDD1B T-Cube LED driver (ThorLabs, Newton, NJ). To compare input bias onto CRF+ and CRF− neurons, input/output curves were generated by incrementally stepping the light intensity at fixed values set along the LED driver and averaging the oEPSC amplitude at each step across 5 sweeps while keeping light exposure constant (5ms). Fixed light-density values correspond to the following intensity steps listed in figures (in mW/mm^2): 1) 0.2, 2) 0.4, 3) 0.6, 4) 1.4, 5) 2.6, and 6) 3.0. Due to the close proximity of the BLA to the CeA, we controlled for transient infection of ChR2 in CeL neurons from occasional viral spread past the intermediate capsule by performing a 200ms light pulse prior to experimentation. Neuronal pairs that demonstrated a prolonged ChR2-mediated inward current were discarded. For some paired INS projection experiments, we manually turned down the exposure time of light until stimulation would not reliably evoke sodium channel currents via voltage-clamp escape. For TTX experiments, light intensity and exposure was kept constant at maximum values used for data collection (3.0 mW/mm^2, and 5ms exposure time), and TTX (500nM) was bath applied after a 5 min baseline recording. For measurements of aEPSCs we replaced extracellular calcium with 4mM strontium and kept maximum stimulation (3.0 mW/mm^2, and 5ms exposure time) constant across conditions. Measurements of aEPSCs were captured in a 500ms window 50ms following onset of the light stimulus. To further assess changes in presynaptic release probability, we manually adjusted stimulation intensity to provide adequate voltage clamping and minimize space

clamp error of oEPSCs from BLA-CeL synapses and measured PPR (oEPSC2/oEPSC1) at various inter-stimulus intervals (ISIs; 25ms, 50ms, 100ms, and 200ms). From the same neurons, AMPAR/NMDAR ratios were calculated by keeping light intensity and exposure time constant between neighboring neurons and measuring the AMPAR-mediated current when voltage-clamping at −70mV for 10 sweeps followed by the same stimulation while voltage clamping at +40mV for the dual component AMPAR and NMDAR-mediated current. The magnitude of the NMDAR-mediated current was calculated at 20ms following the onset of stimulation, when the average AMPAR responses at −70mV had decayed from 95% to 5% of its peak value back to baseline holding current.

For output mapping, CRF-IRES-Cre, CRF-IRES-Cre::Ai14, or SOM-IRES-Cre mice were bilaterally injected with AAV5-EF1α-DIO-ChR2(H134R)-eYFP into the CeA. Mice were allowed to recover for 6-8 weeks for maximal virus expression and entire brains were sectioned and examined for eYFP terminal expression. In separate mice, whole-cell recordings were isolated from brain regions reliably demonstrating a moderate to high degree of YFP expression downstream of the CeA (the CeL, CeM, BNST, PBN, and PAG) and were patched where YFP expression was visibly highest in the slice. Whole-cell recordings were conducted using a high-chloride based internal solution, containing (in mM): 106 K+-gluconate, 40 KCl, 10 HEPES, 4 MgATP, 0.3 Na-GTP, and 20 Na-phosphocreatine (pH 7.20-7.25). Neurons were voltage clamped at −70mV in the presence of AMPA and NMDA receptor blockers CNQX (20μM) and APV (50μM), respectively, so as to isolate GABA dependent currents. Cells that lacked time-locked oIPSCs were scored as non-responsive, and cells that demonstrated time-locked oIPSCS were scored as responsive. To test for $GABA_A$-mediated responses, picrotoxin was bath applied to the perfusate (50μM).

Ex vivo DREADD validation.

To test for the efficacy of DREADDs in regulating the excitability of infected neurons, we performed whole-cell patch clamp recordings from mCherry+ cells in the CeL of DREADD injected animals. Neurons were kept in current clamp configuration and CNO (10μM, Cayman Chemical, Ann Arbor, MI) was bath applied to the slice while the resting membrane potential was monitored for 10min. CNO was applied to the slice after a 3min baseline recording of the resting membrane potential. The average change in resting membrane potential for hM3D(Gq)-infected neurons was calculated to the Vm value at which neurons reached threshold for action potential firing. For hM4D(Gi)-infected neurons, current was injected to keep cells near action potential threshold at a low spontaneous firing frequency (~1Hz) and decreases in action potential frequency were monitored following bath application of CNO.

For experiments examining the presence of CRF-mediated plasticity or release, we recorded sEPSCs from CeL neurons in the presence of picrotoxin (25μM) for a baseline of 3 min followed by bath application of CRF (300nM) or VEH while sEPSCs were monitored for 15 min. In separate experiments, we recorded CRF− neurons in the CeL (mCherry-) of CRF-IRES-Cre mice expressing hM3D(Gq)-infected neurons, and repeated the same analysis while bath applying CNO (10μM) or VEH and monitoring sEPSCs for 20 min. Cells in

which the access resistance fluctuated more than 20% of the baseline during recording were excluded from analysis.

For hM4D(Gi)-mediated inhibition of the BLA to CeL pathway, indiscriminate voltage clamp recordings were made from CeL neurons in the presence of picrotoxin (25μM), and oEPSCs were evoked at 0.1 Hz for a baseline of 5min followed by a 20min bath application of CNO (10μM). Access resistance was monitored throughout experiments by injection of a 5mV hyperpolarizing current, and cells in which the access resistance fluctuated more than 20% of the baseline were discarded from analysis. Data from global hM4D(Gi) and ChR2 expression in the BLA, and mice with Cre-dependent hM4D(Gi) and ChR2 pathway specific expression were pooled for analysis.

Behavioral experiments using DREADDs.

Mice were allowed to recover for 5 weeks to allow maximal DREADD expression in the CeL or BLA. For DREADD-mediated inhibition of BLA-CeL plasticity, mice were allowed to recover for 4 weeks before undergoing behavioral manipulation and whole-cell recordings. For all DREADD experiments, CNO (10mg/kg) was administered 30min prior to behavioral testing, as outlined in figures.

Randomization and inclusion/exclusion criteria.

Mice were selected at random and without bias from group housed cages and assigned to each treatment group for electrophysiology experiments. For behavioral experiments, mice were pseudorandomly assigned to VEH or CNO groups in alternating pairs to best control for age and experiments were run by alternating between treatment groups (running pairs of mice at the same time in identical fear conditioning chambers to control for time of day). Mice in behavioral tests were excluded from analysis only when they exhibited signs of serious behavioral abnormalities (i.e. extreme lethargy accompanied with akinesia) or if they demonstrated missed bilateral injections of target structures. For electrophysiology experiments, outliers were removed as determined by Grubbs or ROUT test. Cells were excluded from analysis if they showed >20% increase in access resistance during the course of an experiment.

Statistical Analysis.

Statistical analyses were conducted using GraphPad Prism 6.0 software. All statistical tests used are reported where they appear in the figure legends. We assumed normality and equal variance for each data set unless otherwise noted, but normality was not formally tested. Comparisons of means between two groups were conducted using one-tailed or two-tailed student’s t-test, where appropriate. One-way or two-way analysis of variance (ANOVA) was used to compare data from multiple experimental groups with post-hoc Holm-Sidaks’s multiple comparisons. Nonparametric tests were used for comparing differences in the mean ratios of maximal current amplitudes from dual-patch recordings, as they may not follow normal distributions[20]. For non-parametric analyses involving comparisons between two groups, Mann-Whitney tests were used, and for comparisons between three groups Kruskill-Wallace tests were used with post-hoc Dunn’s test. Maximal current amplitudes from pairs of neurons were tested for non-linear deviation (hypothetical value of slope=1) using Extra

sum-of-squares F test with the data-fitted slope constrained through the origin. Data collection and analysis was not performed blind to the conditions of the experiments, but analyses were conducted by automated software. No statistical methods were used to pre-determine sample sizes but our sample sizes are similar to those reported in previous publications[1,9,13,20].

Extended Data

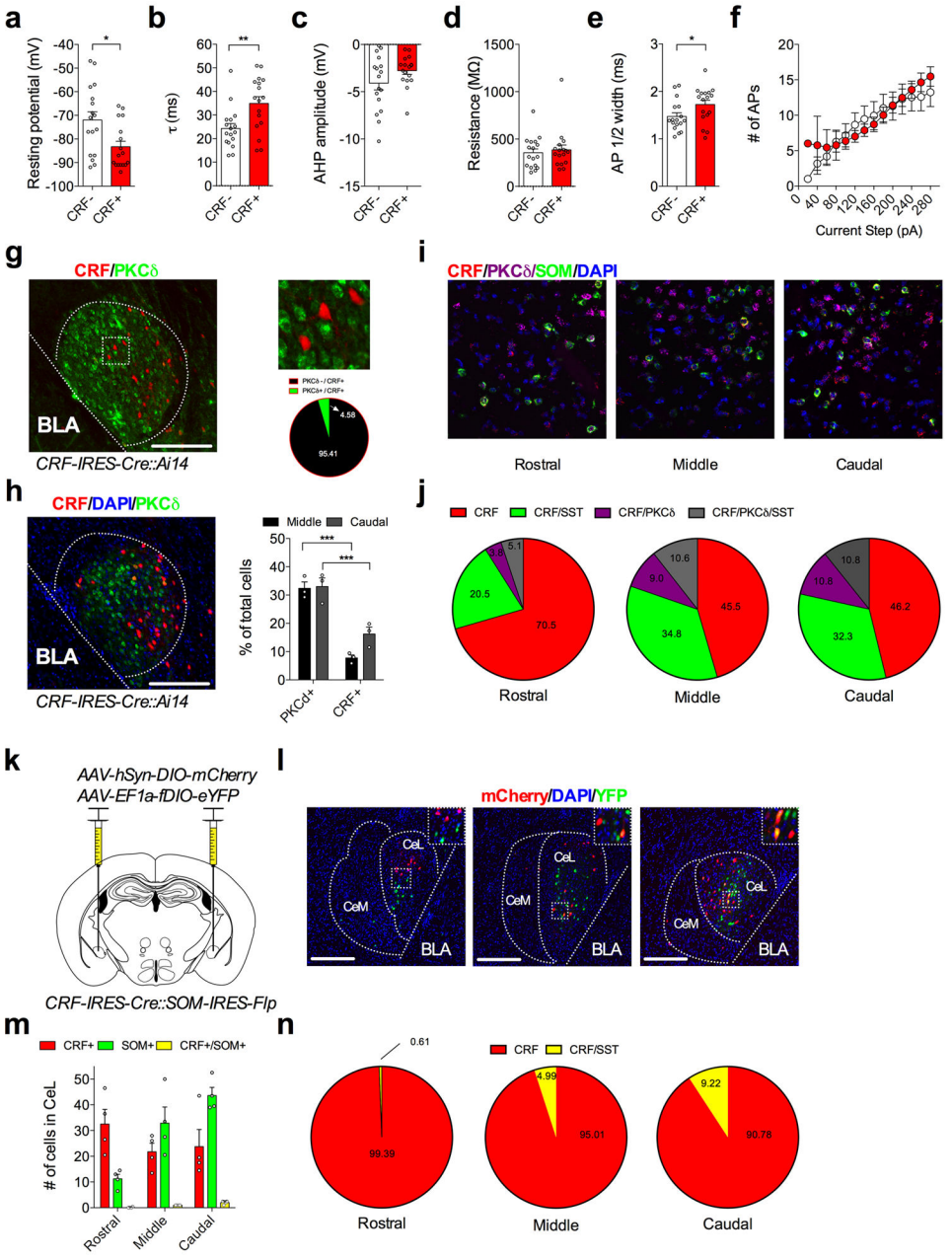

Extended Data Fig. 1. Characterization of CRF+ neurons in the CeL.

a, Resting membrane potential of neighboring CRF+ and CRF− neurons (n=17 cells per group, 4 mice; two-tailed unpaired t-test, $t_{(32)}$=2.682, P=0.0115). **b,** Time constant of neighboring CRF+ and CRF− neurons (n=17 cells per group; two-tailed unpaired t-test, $t_{(32)}$=3.025, P=0.0049). **c,** Afterhyperpolarization amplitude of neighboring CRF+ and CRF − neurons (n=17 cells per group). **d,** Input resistance of neighboring CRF+ and CRF− neurons (n=17 cells per group). **e,** Action potential half-width of neighboring CRF+ and CRF− neurons (n=17 cells per group; two-tailed unpaired t-test, $t_{(32)}$=2.098, P=0.0439). **f,** Number of action potentials per current injection of neighboring CRF+ and CRF− neurons (n=17 cells per group). **g,** Left: image showing immunohistochemical analysis of PKCδ

overlap with CRF+ neurons (scale bar 250μm). Top-right: close up inlet of image on left. Bottom-right: percentage overlap of CRF+ and PKCδ+ neurons (n=4 mice). **h,** Image demonstrating immunohistochemical analysis of PKCδ and CRF+ neurons in the CeA with DAPI stain for quantification of total neurons in CeL. Right: percent of PKCδ+ and CRF+ neurons in the CeL along the rostrocaudal axis (note that PKCδ staining of cell somata was absent in anterior CeL; n=3 mice; two-way ANOVA, $F_{(1,8)}$=80.08, P<0.0001 for rostrocaudal axis; post-hoc Holm-Sidak's multiple comparisons, P=0.0001 for PKCδ and P=0.0009 for CRF+). **i,** Images of fluorescent *in situ* hybridization for CRF, SOM, and PKCδ mRNA in the CeL. Images are pseudocolored for consistency with CRF+ neurons depicted as red throughout figures; *in situ* hybridization along the rostrocaudal axis was independently repeated in n=3 mice. **j,** Percentage overlap of SOM and PKCδ with CRF in the CeL along the rostrocaudal axis (n=3 mice). **k,** Injection strategy for targeting fluorophore expression to CRF and SOM neurons in the CeA. **l,** Representative images of the rostral, middle, and caudal CeA. YFP signal indicates SOM+ neurons, and mCherry signal indicates CRF+ neurons (inlet indicates either the presence or absence of co-localization between YFP and mCherry; scale bars 200μm); viral expression along the rostrocaudal axis was independently repeated in n=4 mice. **m**, Average quantity of CRF+, SOM+, and co-labeled CRF+/SOM+ neurons in the CeL along the rostrocaudal axis (n=4 mice). **n,** Average percentage of co-labeled CRF+/SOM+ neurons in the CeL along the rostrocaudal axis (n=4 mice). Action potentials per current injection are presented as mean ± S.E.M., and bar graphs are presented as mean + S.E.M. *P<0.05, **P<0.01, ***P<0.001.

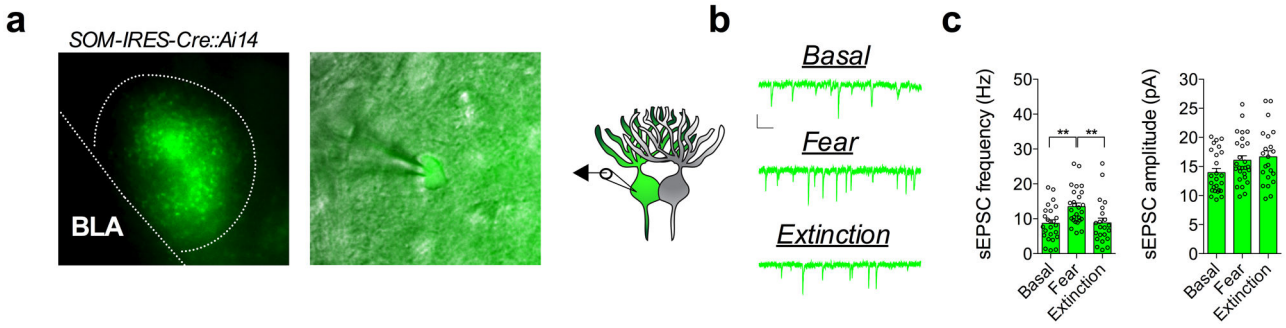

Extended Data Fig. 2. Fear conditioning and extinction training bidirectionally remodel excitatory input onto SOM+ neurons.

a, Left: image of fluorescent SOM+ neurons in the CeL from a coronal slice used in recordings (pseudocolored in green). Middle: DIC and fluorescent overlay of patch-clamp recording from a SOM+ neuron. Right: recording schematic of SOM+ neuron in the CeL; native fluorescence was verified in n=3 slices from a single mouse. **b,** Traces of sEPSC recordings from SOM+ neurons across behavioral conditions (scale bar 100ms, and 10pA). **c,** Average sEPSC frequency and amplitude of SOM+ neurons from naïve (basal), fear conditioned, and fear extinction mice (n=25 basal, 3 mice, n=27 fear, 4 mice, n=22 extinction cells, 3 mice; one-way ANOVA, $F_{(2,71)}$=0.1380, P=0.0030; post-hoc Holm-Sidak's multiple comparisons, basal vs. fear P=0.0051, fear vs. extinction P=0.0051). Bar graphs are presented as mean + S.E.M. **P<0.01.

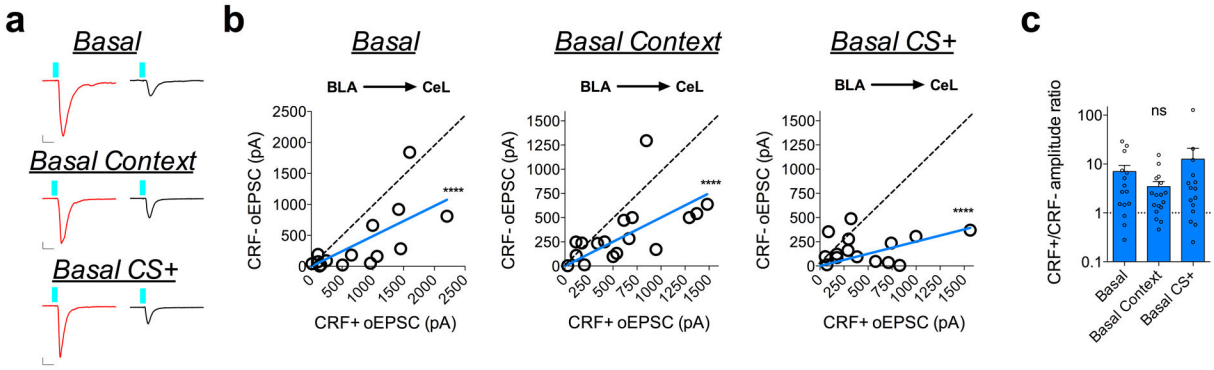

Extended Data Fig. 3. Conditioning context or CS exposure does not affect BLA-CeL circuit input bias onto CRF+ and CRF− neurons.

a, Traces of maximal oEPSC amplitude from CRF+ (red) and CRF− (black) neuronal pairs across behavioral conditions for stimulation of the BLA-CeL circuit (scale bars 10ms, 100pA). **b,** XY graphs depicting skew-plot of maximal oEPSC amplitude from each CRF+ and CRF− neuronal pair for behavioral conditions (n=15 basal pairs, 4 mice, n=17 basal context pairs, 4 mice, and n=15 basal CS+ pairs, 5 mice; extra sum-of-squares F test, $F_{(1,14)}$=30.55, P<0.0001 for basal, $F_{(1,16)}$=35.56, P<0.0001 for basal context, and $F_{(1,14)}$=113.2, P<0.0001 for basal CS+). **c,** Representation of CRF+ and CRF− maximal oEPSC amplitude ratio (log scale; n=14 basal pairs, n=17 basal context, and n=14 basal CS+ pairs; Kruskal-Wallis test, ns=non-significant, P=0.5860). XY skew-plots are presented as absolute value. Bar graphs are presented as mean + S.E.M. ****P<0.0001.

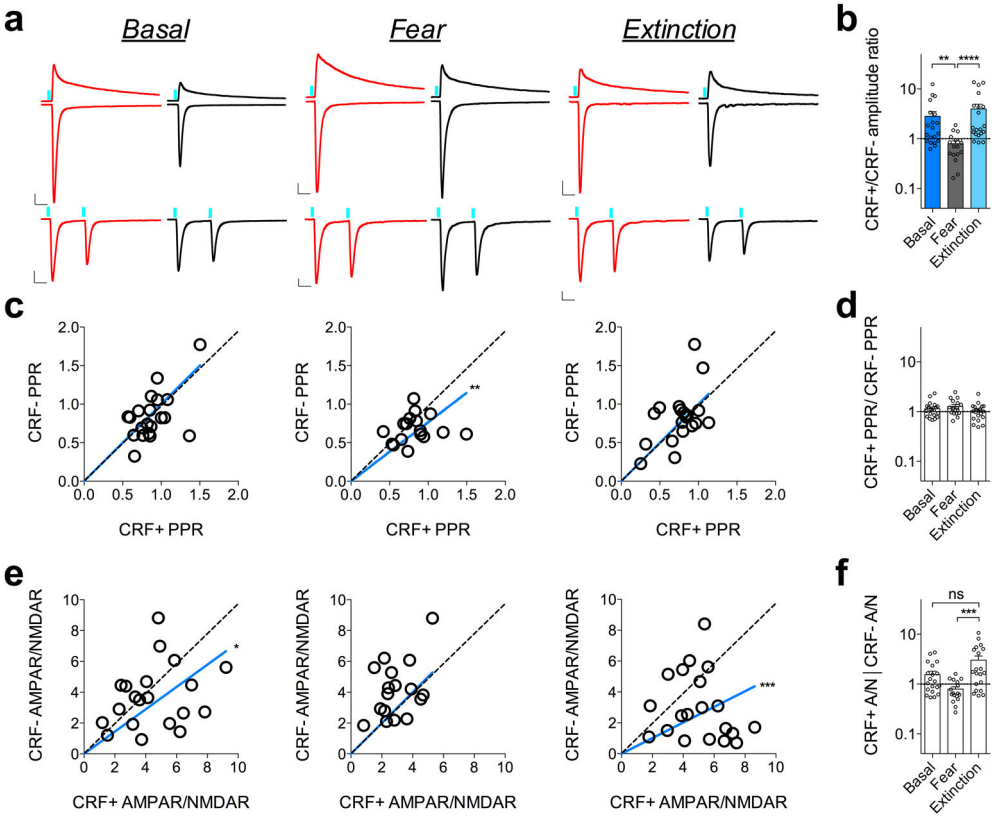

Extended Data Fig. 4. Experience-dependent remodeling of BLA-CeL input bias is associated with postsynaptic alterations but not changes in presynaptic release probability.

a, Traces of AMPAR/NMDAR ratios and PPR from neighboring CRF+ and CRF− neurons following stimulation of the BLA-CeL circuit (scale bars 20ms, 200pA). **b,** Representation of CRF+ and CRF− maximal oEPSC amplitude ratio (log scale; n=20 basal pseudopairs, n=17 fear pseudopairs, and n=20 extinction pseudopairs; Kruskal-Wallis test, P<0.0001; post-hoc Dunn's multiple comparisons, basal vs. fear P=0.0025, fear vs. extinction P<0.0001). **c,** XY graphs depicting skew-plot of PPR from neighboring CRF+ and CRF− neurons across behavioral conditions (n=20 basal pseudopairs, 5 mice, n=17 fear pseudopairs, 5 mice, and n=20 extinction pseudopairs, 5 mice; extra sum-of-squares F test, $F_{(1,16)}$=11.29, P=0.0040 for fear). **d,** Representation of the ratio of PPR between neighboring CRF+ and CRF− neurons (log scale; n=20 basal pairs, n=17 fear pairs, and n=20 extinction pairs). **e,** XY graphs depicting skew-plot of AMPAR/NMDAR from neighboring CRF+ and CRF− neurons across behavioral conditions (n=20 basal pseudopairs, 5 mice, n=17 fear pseudopairs, 5 mice, and n=20 extinction pseudopairs, 5 mice; extra sum-of-squares F test, $F_{(1,19)}$=7.374, P=0.0137 for basal, and $F_{(1,19)}$=20.89, P=0.0002 for extinction). **f,** Representation of the ratio of AMPAR/NMDAR between neighboring CRF+ and CRF− neurons (log scale; n=20 basal pseudopairs, n=17 fear pseudopairs, and n=20 extinction pseudopairs; Kruskal-Wallis test, P=0.0013; post-hoc Dunn's multiple comparisons, fear vs. extinction P=0.0008, ns=not significant, P=0.3683). XY skew-plots are presented as absolute value. Bar graphs are presented as mean + S.E.M. *P<0.05, **P<0.01, ***P<0.001, ****P<0.0001.

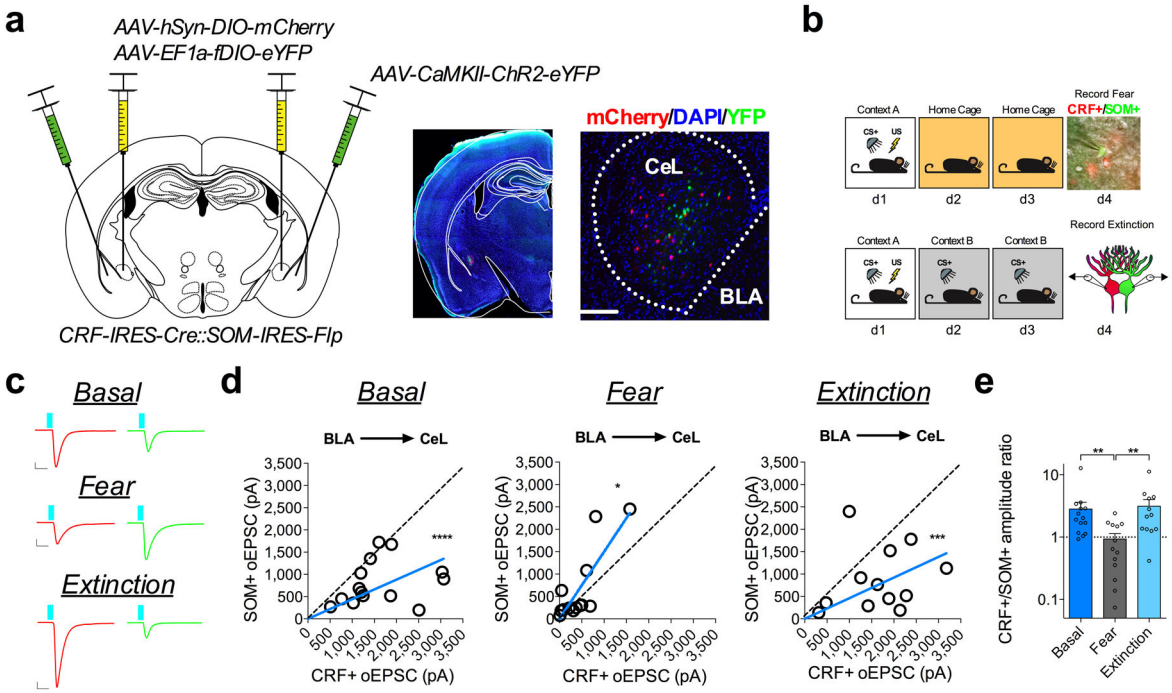

Extended Data Fig. 5. Fear conditioning and extinction training bidirectionally remodel the BLA-CeL circuit input bias onto CRF+ and SOM+ neurons.

a, Left: optogenetic circuit mapping approach with viral injection. Right: image of YFP and mCherry expression in SOM+ and CRF+ neurons (image is from an animal with no injection of ChR2 expression in the BLA for clarity of fluorophore expression in adjacent CeA; scale bar 175μm); viral expression was independently verified and repeated in n=4 mice. **b,** Experimental paradigm for dual patch-clamp recordings from CRF+ and SOM+ neurons in fear conditioned and fear extinguished mice. Bottom-right: DIC and fluorescent overlay image of dual-patch clamp recording from CRF+ and SOM+ pair. **c,** Traces of maximal oEPSC amplitude from CRF+ (red) and SOM+ (green) neuronal pairs across behavioral conditions for stimulation of the BLA-CeL circuit (scale bars 10ms, 200pA). **d,** XY graphs depicting skew-plot of maximal oEPSC amplitude from each CRF+ and SOM+ neuronal pair for behavioral conditions (n=14 basal pairs, 5 mice, n=13 fear pairs, 6 mice, and n=12 extinction pairs, 5 mice; extra sum-of-squares F test, $F_{(1,13)}$=47.34, P<0.0001 for basal, $F_{(1,12)}$=5.444, P=0.0378 for fear, and $F_{(1,11)}$=21.16, P=0.0008 for extinction). **e,** Representation of CRF+/CRF− maximal oEPSC amplitude ratio (log scale; n=14 basal pairs, n=13 fear pairs, and n=12 extinction pairs; Kruskal-Wallis test, P=0.0042; post-hoc Dunn's multiple comparisons, basal vs. fear P=0.0091, fear vs. extinction P=0.0076). XY skew-plots are presented as absolute value. Bar graphs are presented as mean + S.E.M. *P<0.05, **P<0.01, ***P<0.001, ****P<0.0001.

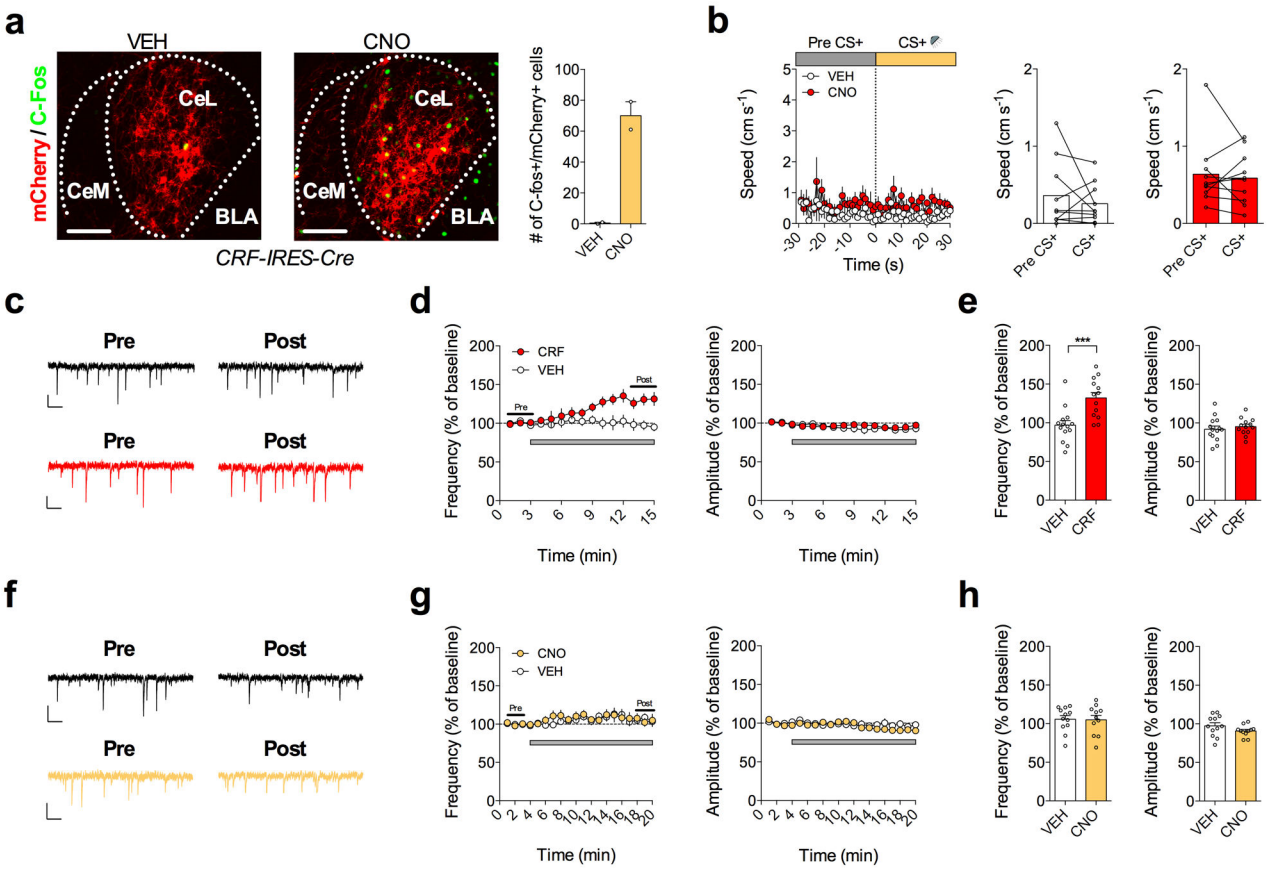

Extended Data Fig. 6. Gαq-coupled-DREADD excites CRF+ neurons but does not mimic the effects of exogenous CRF on glutamatergic transmission.

a, Left: images representing immunohistochemical analysis of immediate early gene c-Fos in *CRF-IRES-Cre* mice expressing cre-dependent hM3D(Gq)-mCherry in the CeL, followed by systemic administration of VEH or CNO (scale bar 200μm). Right: quantification of c-Fos+ neurons overlapping with hM3D(Gq)-mCherry+ neurons in the CeL (n=2 mice per group). **b,** Average time-locked speed trace during early fear memory recall phase for mice injected with VEH or CNO (first 5 CS+ presentations on extinction session 1 day 2 (d2)) from the same mice in experiment presented in Fig. 7f,g (n=10 mice per group). **c,** Representative traces of sEPSCs from CeL neurons before (pre) and after (post) VEH or CRF application (scale bars 100ms, 10pA). **d,** Effects of VEH or CRF bath application on sEPSC frequency and amplitude over time (gray bar indicates application of CRF or VEH, n=14 VEH neurons, 5 mice, n=13 CNO neurons, 5 mice). **e,** Summary of sEPSC frequency and amplitude after application of VEH or CRF (n=14 VEH neurons, 5 mice, n=13 CNO neurons, 5 mice; two-tailed unpaired t-test, $t_{(25)}$=3.818, P=0.0008). **f,** Representative traces of sEPSCs from CeL neurons before (pre) and after (post) VEH or CNO application in mice expressing hM3D(Gq)-mCherry in CRF+ neurons of the CeL (scale bars 100ms, 10pA). **g,** Effects of VEH or CNO bath application on sEPSC frequency and amplitude over time in mice expressing hM3D(Gq)-mCherry in CRF+ neurons of the CeL (gray bar indicates application of CNO or VEH, n=12 VEH neurons, 5 mice, n=11 CNO neurons, 5 mice). **h,** Summary of sEPSC frequency and amplitude after application of VEH or CNO in mice

expressing hM3D(Gq)-mCherry in CRF+ neurons of the CeL (n=12 VEH neurons, 5 mice, n=11 CNO neurons, 5 mice). Effects of CRF on sEPSC frequency or amplitude over time are presented as mean ± S.E.M., and bar graphs are presented as mean + S.E.M. *P<0.05, ***P<0.001.

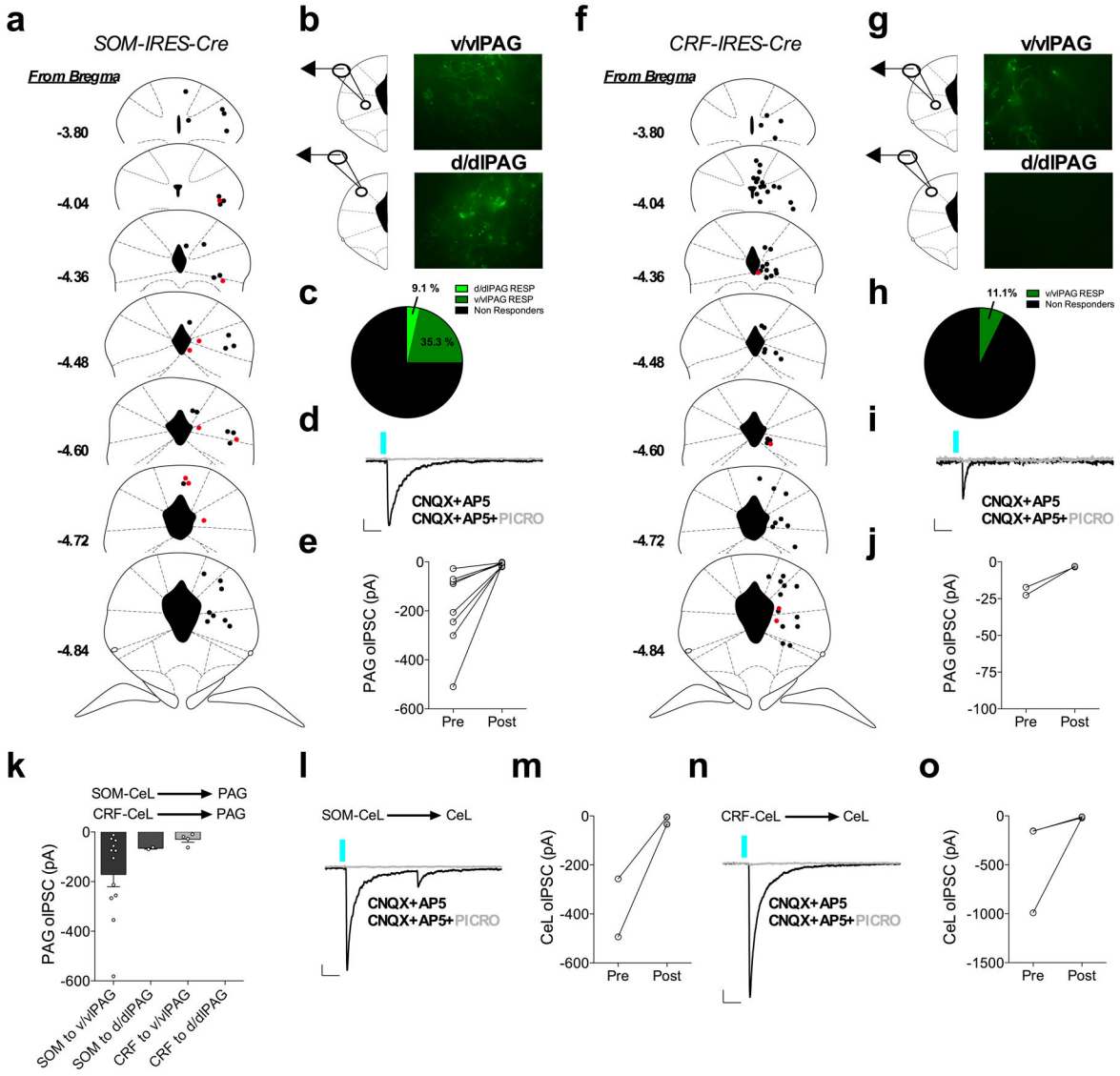

Extended Data Fig. 7. CRF+ and SOM+ neurons in the CeA signal through long-range and local GABAergic synapses to the PAG and CeL.

a, Recording sites for long-range projections of SOM+ CeA neurons to the PAG. Red dots indicate responsive neurons demonstrating oIPSCs following ChR2 stimulation of axon terminals, and black dots indicate non-responsive neurons. **b,** Fluorescent images taken from slice recordings demonstrating the presence of ChR2-eYFP terminals in the ventral/ventrolateral PAG and the dorsal/dorsolateral PAG; location of terminals was independently verified and repeated in n=4 mice. **c,** Connectivity index indicating percentage of responsive and non-responsive PAG neurons from SOM+ input (n=56 neurons, 4 mice; RESP=responsive neurons). **d,** Example trace of time-locked oIPSC recorded from a responsive neuron in the PAG, which was blocked following application of picrotoxin (scale bars 20ms, 20pA). **e,** Summary of oIPSCs blocked by picrotoxin in the PAG (n=8 neurons, 4 mice). **f,** Recording sites for long-range projections of CRF+ CeA neurons to the PAG. Red dots indicate responsive neurons demonstrating oIPSCs following ChR2 stimulation of axon

terminals, and black dots indicate non-responsive neurons. **g,** Fluorescent images taken from slice recordings demonstrating the presence of ChR2-eYFP terminals in the ventral/ventrolateral PAG and lack of terminals in the dorsal/dorsolateral PAG; location of terminals was independently verified and repeated in n=4 mice. **h,** Connectivity index indicating percentage of responsive and non-responsive PAG neurons from CRF+ input (n=62 neurons, 4 mice; RESP=responsive neurons). **i,** Example trace of time-locked oIPSC recorded from a responsive neuron in the PAG, which was blocked following application of picrotoxin (scale bars 20ms, 20pA). **j,** Summary of oIPSCs blocked by picrotoxin in the PAG (n=2 neurons, 2 mice). **k,** Average amplitude of oIPSCs from SOM+ and CRF+ neuronal projections to the PAG (n=14 neurons, 4 mice for SOM+ input, n=2 neurons, 4 mice for CRF+ input). **l,** Example trace of time-locked oIPSC recorded from a SOM-responsive neuron in the CeL, which was blocked following application of picrotoxin (scale bars 20ms, 50pA). **m,** Summary of oIPSCs blocked by picrotoxin in the CeL (n=2 neurons, 2 mice). **n,** Example trace of time-locked oIPSC recorded from a CRF− responsive neuron in the CeL, which was blocked following application of picrotoxin (scale bars 20ms, 100pA). **o,** Summary of oIPSCs blocked by picrotoxin in the CeL (n=3 neurons, 3 mice). Bar graphs are presented as mean + S.E.M.

Supplementary Material

Refer to Web version on PubMed Central for supplementary material.

ACKNOWLEDGMENTS

This work was supported by NIH grants MH107435 and AA26186 (S.P.), F31 MH111103 (N.D.H), and DA042475 and AA019455 (D.G.W). Imaging of ChR2 expression in the CeL and in situ hybridization was performed in part through the use of the Vanderbilt Cell Imaging Shared Resource center. We thank Robert Matthews for training lab personnel for use of confocal microscopes in this study.

REFERENCES

1. Li H et al. Experience-dependent modification of a central amygdala fear circuit. Nature neuroscience 16, 332–339, doi:10.1038/nn.3322 (2013). [PubMed: 23354330]
2. Fadok JP et al. A competitive inhibitory circuit for selection of active and passive fear responses. Nature 542, 96–100, doi:10.1038/nature21047 (2017). [PubMed: 28117439]
3. Douglass AM et al. Central amygdala circuits modulate food consumption through a positive-valence mechanism. Nature neuroscience 20, 1384–1394, doi:10.1038/nn.4623 (2017). [PubMed: 28825719]
4. Amir A, Lee SC, Headley DB, Herzallah MM & Pare D Amygdala Signaling during Foraging in a Hazardous Environment. The Journal of neuroscience : the official journal of the Society for Neuroscience 35, 12994–13005, doi:10.1523/JNEUROSCI.0407-15.2015 (2015). [PubMed: 26400931]
5. Han W et al. Integrated Control of Predatory Hunting by the Central Nucleus of the Amygdala. Cell 168, 311–324 e318, doi:10.1016/j.cell.2016.12.027 (2017). [PubMed: 28086095]
6. Do Monte FH, Quirk GJ, Li B & Penzo MA Retrieving fear memories, as time goes by. Molecular psychiatry 21, 1027–1036, doi:10.1038/mp.2016.78 (2016). [PubMed: 27217148]
7. Maren S Neurobiology of Pavlovian fear conditioning. Annual review of neuroscience 24, 897–931, doi:10.1146/annurev.neuro.24.1.897 (2001).
8. Duvarci S & Pare D Amygdala microcircuits controlling learned fear. Neuron 82, 966–980, doi:10.1016/j.neuron.2014.04.042 (2014). [PubMed: 24908482]

9. Penzo MA et al. The paraventricular thalamus controls a central amygdala fear circuit. Nature 519, 455–459, doi:10.1038/nature13978 (2015). [PubMed: 25600269]
10. Ciocchi S et al. Encoding of conditioned fear in central amygdala inhibitory circuits. Nature 468, 277–282, doi:10.1038/nature09559 (2010). [PubMed: 21068837]
11. Haubensak W et al. Genetic dissection of an amygdala microcircuit that gates conditioned fear. Nature 468, 270–276, doi:10.1038/nature09553 (2010). [PubMed: 21068836]
12. Duvarci S, Popa D & Pare D Central amygdala activity during fear conditioning. The Journal of neuroscience : the official journal of the Society for Neuroscience 31, 289–294, doi:10.1523/JNEUROSCI.4985-10.2011 (2011). [PubMed: 21209214]
13. Sanford CA et al. A Central Amygdala CRF Circuit Facilitates Learning about Weak Threats. Neuron 93, 164–178, doi:10.1016/j.neuron.2016.11.034 (2017). [PubMed: 28017470]
14. Asok A et al. Optogenetic silencing of a corticotropin-releasing factor pathway from the central amygdala to the bed nucleus of the stria terminalis disrupts sustained fear. Molecular psychiatry 23, 914–922, doi:10.1038/mp.2017.79 (2018). [PubMed: 28439099]
15. McCall JG et al. CRH Engagement of the Locus Coeruleus Noradrenergic System Mediates Stress-Induced Anxiety. Neuron 87, 605–620, doi:10.1016/j.neuron.2015.07.002 (2015). [PubMed: 26212712]
16. Kim J, Zhang X, Muralidhar S, LeBlanc SA & Tonegawa S Basolateral to Central Amygdala Neural Circuits for Appetitive Behaviors. Neuron 93, 1464–1479 e1465, doi:10.1016/j.neuron.2017.02.034 (2017). [PubMed: 28334609]
17. Gafford GM & Ressler KJ GABA and NMDA receptors in CRF neurons have opposing effects in fear acquisition and anxiety in central amygdala vs. bed nucleus of the stria terminalis. Hormones and behavior 76, 136–142, doi:10.1016/j.yhbeh.2015.04.001 (2015). [PubMed: 25888455]
18. Botta P et al. Regulating anxiety with extrasynaptic inhibition. Nature neuroscience 18, 1493–1500, doi:10.1038/nn.4102 (2015). [PubMed: 26322928]
19. Yu K et al. The central amygdala controls learning in the lateral amygdala. Nature neuroscience 20, 1680–1685, doi:10.1038/s41593-017-0009-9 (2017). [PubMed: 29184202]
20. MacAskill AF, Cassel JM & Carter AG Cocaine exposure reorganizes cell type- and input-specific connectivity in the nucleus accumbens. Nature neuroscience 17, 1198–1207, doi:10.1038/nn.3783 (2014). [PubMed: 25108911]
21. Nieuwenhuys R The insular cortex: a review. Progress in brain research 195, 123–163, doi:10.1016/B978-0-444-53860-4.00007-6 (2012). [PubMed: 22230626]
22. Berret E et al. Insular cortex processes aversive somatosensory information and is crucial for threat learning. Science, doi:10.1126/science.aaw0474 (2019).
23. Tye KM et al. Amygdala circuitry mediating reversible and bidirectional control of anxiety. Nature 471, 358–362, doi:10.1038/nature09820 (2011). [PubMed: 21389985]
24. Cai H, Haubensak W, Anthony TE & Anderson DJ Central amygdala PKC-delta(+) neurons mediate the influence of multiple anorexigenic signals. Nature neuroscience 17, 1240–1248, doi:10.1038/nn.3767 (2014). [PubMed: 25064852]
25. Han S, Soleiman MT, Soden ME, Zweifel LS & Palmiter RD Elucidating an Affective Pain Circuit that Creates a Threat Memory. Cell 162, 363–374, doi:10.1016/j.cell.2015.05.057 (2015). [PubMed: 26186190]
26. Geddes SD et al. Target-specific modulation of the descending prefrontal cortex inputs to the dorsal raphe nucleus by cannabinoids. Proceedings of the National Academy of Sciences of the United States of America 113, 5429–5434, doi:10.1073/pnas.1522754113 (2016). [PubMed: 27114535]
27. Biane JS, Takashima Y, Scanziani M, Conner JM & Tuszynski MH Thalamocortical Projections onto Behaviorally Relevant Neurons Exhibit Plasticity during Adult Motor Learning. Neuron 89, 1173–1179, doi:10.1016/j.neuron.2016.02.001 (2016). [PubMed: 26948893]
28. Kaeser PS & Regehr WG Molecular mechanisms for synchronous, asynchronous, and spontaneous neurotransmitter release. Annual review of physiology 76, 333–363, doi:10.1146/annurev-physiol-021113-170338 (2014).
29. McGarry LM & Carter AG Prefrontal Cortex Drives Distinct Projection Neurons in the Basolateral Amygdala. Cell reports 21, 1426–1433, doi:10.1016/j.celrep.2017.10.046 (2017). [PubMed: 29117549]

30. Armbruster BN, Li X, Pausch MH, Herlitze S & Roth BL Evolving the lock to fit the key to create a family of G protein-coupled receptors potently activated by an inert ligand. Proceedings of the National Academy of Sciences of the United States of America 104, 5163–5168, doi:10.1073/pnas.0700293104 (2007). [PubMed: 17360345]
31. Anglada-Figueroa D & Quirk GJ Lesions of the basal amygdala block expression of conditioned fear but not extinction. The Journal of neuroscience : the official journal of the Society for Neuroscience 25, 9680–9685, doi:10.1523/JNEUROSCI.2600-05.2005 (2005). [PubMed: 16237172]
32. Tipps M, Marron Fernandez de Velasco E, Schaeffer A & Wickman K. Inhibition of Pyramidal Neurons in the Basal Amygdala Promotes Fear Learning. eNeuro 5, doi:10.1523/ENEURO.0272-18.2018 (2018).
33. Namburi P et al. A circuit mechanism for differentiating positive and negative associations. Nature 520, 675–678, doi:10.1038/nature14366 (2015). [PubMed: 25925480]
34. Tervo DG et al. A Designer AAV Variant Permits Efficient Retrograde Access to Projection Neurons. Neuron 92, 372–382, doi:10.1016/j.neuron.2016.09.021 (2016). [PubMed: 27720486]
35. Gomez JL et al. Chemogenetics revealed: DREADD occupancy and activation via converted clozapine. Science 357, 503–507, doi:10.1126/science.aan2475 (2017). [PubMed: 28774929]
36. Gafford G, Jasnow AM & Ressler KJ Grin1 receptor deletion within CRF neurons enhances fear memory. PloS one 9, e111009, doi:10.1371/journal.pone.0111009 (2014). [PubMed: 25340785]
37. Dedic N et al. Chronic CRH depletion from GABAergic, long-range projection neurons in the extended amygdala reduces dopamine release and increases anxiety. Nature neuroscience 21, 803–807, doi:10.1038/s41593-018-0151-z (2018). [PubMed: 29786085]
38. Tovote P et al. Midbrain circuits for defensive behaviour. Nature 534, 206–212, doi:10.1038/nature17996 (2016). [PubMed: 27279213]
39. Evans DA et al. A synaptic threshold mechanism for computing escape decisions. Nature 558, 590–594, doi:10.1038/s41586-018-0244-6 (2018). [PubMed: 29925954]
40. Pitman RK et al. Biological studies of post-traumatic stress disorder. Nature reviews. Neuroscience 13, 769–787, doi:10.1038/nrn3339 (2012). [PubMed: 23047775]
41. Yu K, Garcia da Silva P, Albeanu DF & Li B Central Amygdala Somatostatin Neurons Gate Passive and Active Defensive Behaviors. The Journal of neuroscience : the official journal of the Society for Neuroscience 36, 6488–6496, doi:10.1523/JNEUROSCI.4419-15.2016 (2016). [PubMed: 27307236]
42. van den Pol AN Neuropeptide transmission in brain circuits. Neuron 76, 98–115, doi:10.1016/j.neuron.2012.09.014 (2012). [PubMed: 23040809]
43. Yeung M, Engin E & Treit D Anxiolytic-like effects of somatostatin isoforms SST 14 and SST 28 in two animal models (Rattus norvegicus) after intra-amygdalar and intra-septal microinfusions. Psychopharmacology 216, 557–567, doi:10.1007/s00213-011-2248-x (2011). [PubMed: 21424237]
44. Yeung M & Treit D The anxiolytic effects of somatostatin following intra-septal and intra-amygdalar microinfusions are reversed by the selective sst2 antagonist PRL2903. Pharmacology, biochemistry, and behavior 101, 88–92, doi:10.1016/j.pbb.2011.12.012 (2012).
45. Kahl E & Fendt M Injections of the somatostatin receptor type 2 agonist L-054,264 into the amygdala block expression but not acquisition of conditioned fear in rats. Behavioural brain research 265, 49–52, doi:10.1016/j.bbr.2014.02.011 (2014). [PubMed: 24548855]
46. Herry C et al. Switching on and off fear by distinct neuronal circuits. Nature 454, 600–606, doi:10.1038/nature07166 (2008). [PubMed: 18615015]
47. McCullough KM et al. Molecular characterization of Thy1 expressing fear-inhibiting neurons within the basolateral amygdala. Nature communications 7, 13149, doi:10.1038/ncomms13149 (2016).
48. Madisen L et al. Transgenic mice for intersectional targeting of neural sensors and effectors with high specificity and performance. Neuron 85, 942–958, doi:10.1016/j.neuron.2015.02.022 (2015). [PubMed: 25741722]
49. Krashes MJ et al. Rapid, reversible activation of AgRP neurons drives feeding behavior in mice. J Clin Invest 121, 1424–1428, doi:10.1172/JCI46229 (2011). [PubMed: 21364278]

50. Hartley ND et al. 2-arachidonoylglycerol signaling impairs short-term fear extinction. Translational psychiatry 6, e749, doi:10.1038/tp.2016.26 (2016). [PubMed: 26926885]

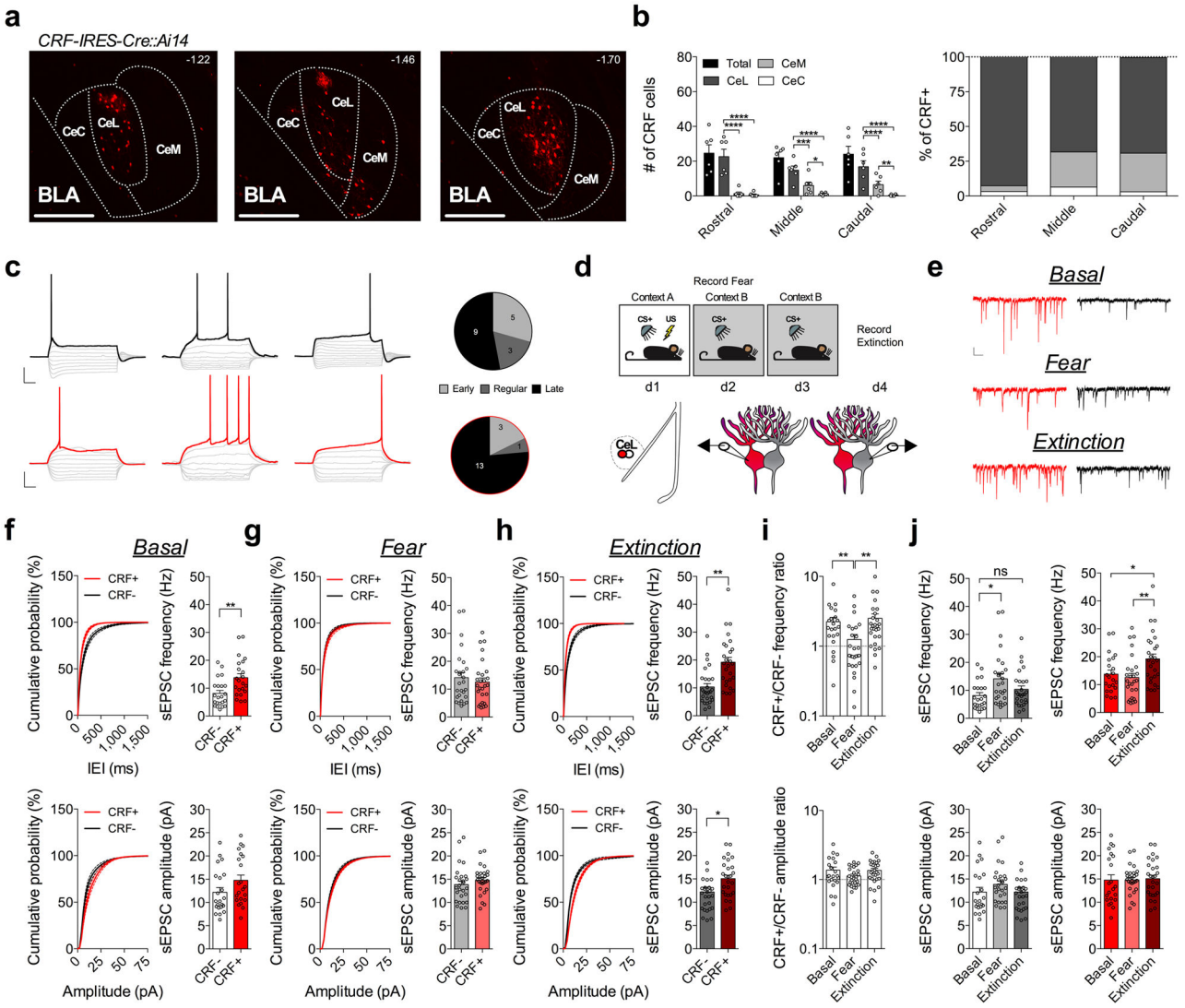

Fig. 1. Fear conditioning and extinction training bidirectionally remodel excitatory input bias onto CRF+ and CRF− CeL neurons.

a, Images depicting CRF+ neuronal distribution across the rostrocaudal axis of the CeA (numbers in top right corner depict distance from bregma; scale bars 250μm). **b,** Number and percentage of CRF+ neurons within each subdivision of the CeA along the rostrocaudal axis (n=6 mice; two-way ANOVA, $F_{(3,15)}$=31.72, P<0.0001 for CeA subdivisions; post-hoc Holm-Sidak's multiple comparisons, Rostral CeL vs. CeM P<0.0001, CeL vs. Cec P<0.0001, Middle CeL vs. CeM P=0.0004, CeL vs. CeC P<0.0001, CeM vs. CeC P=0.0228, Caudal CeL vs. CeM P<0.0001, CeL vs. CeM P<0.0001, CeM vs. CeC P=0.0057). **c,** Left: traces of early, regular, and late firing CRF+ and CRF− neurons. CRF− neuronal traces are depicted with a black outline, and CRF+ with a red outline (scale bars 100ms, and 20mV). Right: total number of early, regular and late firing CRF+ and neighboring CRF− neurons plotted as parts of whole graph (n=17 cells per group, 4 mice). **d,** Experimental paradigm for recording from fear conditioned or fear extinguished mice using alternating patch-clamp technique of neighboring CRF+ and CRF− neurons. **e,** Traces of sEPSC recordings from

neighboring CRF+ and CRF− neurons across behavioral conditions (scale bar 100ms, and 10pA). **f,** Cumulative probability distribution and average sEPSC frequency and amplitude for neighboring CRF+ and CRF− neurons in naïve mice (basal condition) (n=22 cells per group, 5 mice; two-tailed unpaired t-tests, $t_{(42)}$=3.144, P=0.0031 for sEPSC frequency). **g,** Cumulative probability distribution and average sEPSC frequency and amplitude for neighboring CRF+ and CRF− neurons following fear conditioning (n=27 cells per group, 5 mice). **h,** Cumulative probability distribution and average sEPSC frequency and amplitude for neighboring CRF+ and CRF− neurons following fear extinction (n=27 cells per group, 5 mice; two-tailed unpaired t-tests, $t_{(52)}$=4.175, P=0.0001 for sEPSC frequency, $t_{(52)}$=2.226, P=0.0304 for sEPSC amplitude). **i,** Representation of CRF+/CRF− frequency and amplitude ratios from neighboring CRF+ and CRF− neurons across fear states (log scale; n=22 basal pseudopairs, n=27 fear pseudopairs, n=27 extinction pseudopairs; Kruskal-Wallis tests, P=0.0134; post-hoc Dunn's multiple comparisons, basal vs. fear P=0.0049, fear vs. extinction P=0.0011). **j,** Representation of Average sEPSC frequency and amplitude for CRF − (white/grey bars) neurons or CRF+ (red bars) neurons across fear states (n=22 basal, n=27 fear, n=27 extinction cells; one-way ANOVAs, $F_{(2,73)}$=4.295, P=0.0172 for CRF−, $F_{(2,73)}$=5.316, P=0.0070 for CRF+; post-hoc Holm-Sidak's multiple comparisons, CRF− basal vs. fear frequency P=0.0109, CRF− basal vs. extinction frequency P=0.2921, CRF+ basal vs. extinction frequency P=0.0196, CRF+ fear vs. extinction frequency P=0.0057). IEI=inter-event interval, ns=non-significant. Cumulative probability distributions are plotted as mean ± S.E.M., and bar graphs are presented as mean + S.E.M.*P<0.05, **P<0.01, ***P<0.001, ****P<0.0001.

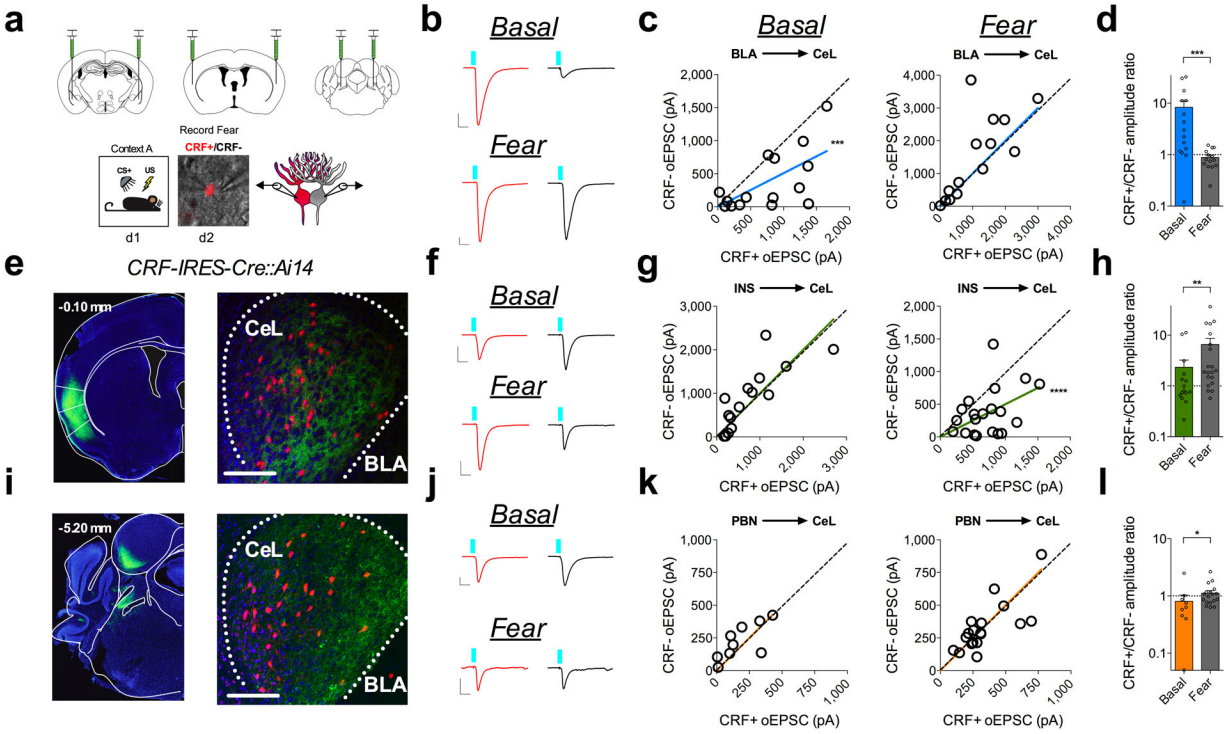

Fig. 2. Fear conditioning remodels circuit specific input bias onto CRF+ and CRF− neurons in the CeL.

a, Optogenetic circuit-mapping approach with viral injections into the BLA, INS, and PBN. Bottom-right: DIC and fluorescent overlay of dual-patch clamp recording from CRF+ and CRF− pair. **b,** Traces of maximal oEPSC amplitude from CRF+ (red) and CRF− (black) neuronal pairs across behavioral conditions for stimulation of the BLA-CeL circuit (scale bars 10ms, 200pA). **c,** XY graphs depicting skew-plot of maximal oEPSC amplitude from each CRF+ and CRF− neuronal pair for behavioral conditions (n=15 basal pairs, 5 mice, n=14 fear pairs, 5 mice; extra sum-of-squares F test, $F_{(1,14)}$=25.61, P=0.0002 for basal). **d,** Representation of CRF+/CRF− maximal oEPSC amplitude ratio (log scale; n=15 basal pairs, n=14 fear pairs; two-tailed Mann-Whitney test, P=0.0005). **e,** Image of ChR2-eYFP expression in the INS (number in top left corner depicts distance from bregma), and eYFP-positive terminals in the CeL (scale bar 150μm); location of terminals was independently verified and repeated in n=4 mice. **f,** Traces of maximal oEPSC amplitude from CRF+ (red) and CRF− (black) neuronal pairs across behavioral conditions for stimulation of the INS-CeL circuit (scale bars 10ms, 200pA). **g,** XY graphs depicting skew-plot of maximal oEPSC amplitude from each CRF+ and CRF− neuronal pair for behavioral conditions (n=15 basal pairs, 5 mice, n=20 fear pairs, 5 mice; extra sum-of-squares F test, $F_{(1,19)}$=28.72, P<0.0001). **h,** Representation of CRF+/CRF− maximal oEPSC amplitude ratio (log scale; n=15 basal pairs, n=20 fear pairs; two-tailed Mann-Whitney test, P=0.0076). **i,** Image of ChR2-eYFP expression in the PBN (number in top left corner depicts distance from bregma), and eYFP-positive terminals in the CeL (scale bar 150μm); location of terminals was independently verified and repeated in n=3 mice. **j,** Traces of maximal oEPSC amplitude from CRF+ (red) and CRF− (black) neuronal pairs across behavioral conditions for stimulation of the PBN-CeL circuit (scale bars 10ms, 100pA). **k,** XY graphs depicting skew-plot of maximal oEPSC

amplitude from each CRF+ and CRF− neuronal pair for behavioral conditions (n=9 basal pairs, 5 mice, n=19 fear pairs, 4 mice). **l,** Representation of CRF+/CRF− maximal oEPSC amplitude ratio (log scale; n=9 basal pairs, n=18 fear pairs; two-tailed Mann-Whitney test, P=0.0196). XY skew-plots are presented as absolute value. Bar graphs are presented as mean + S.E.M. *P<0.05, **P<0.01, ***P<0.001, ****P<0.0001.

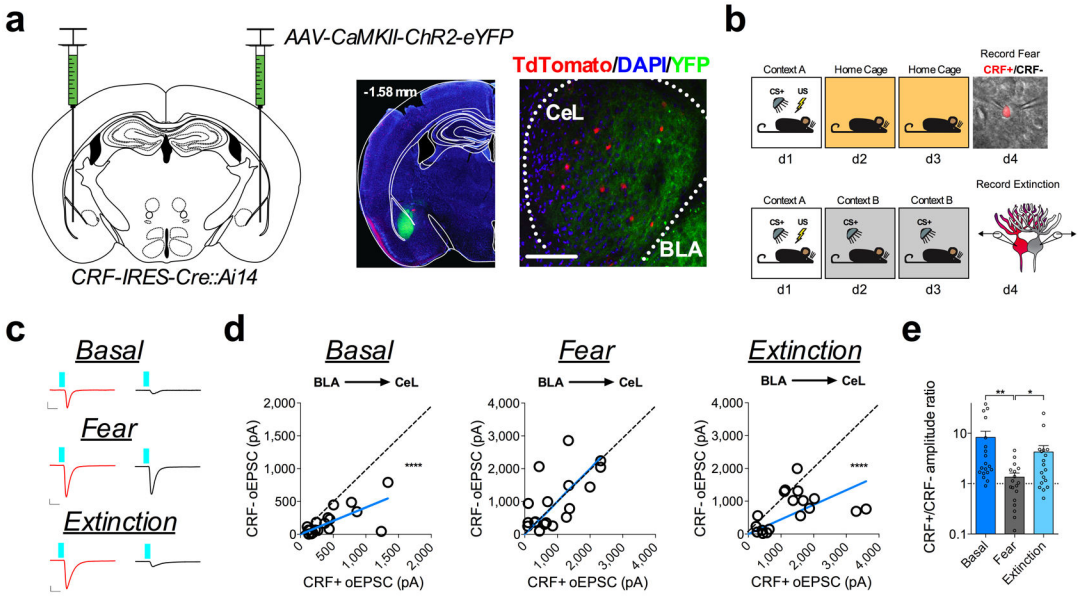

Fig. 3. Fear conditioning and extinction training bidirectionally remodel the BLA-CeL circuit input bias onto CRF+ and CRF− neurons.

a, Left: optogenetic circuit mapping approach with viral injection. Right: image of ChR2-eYFP expression in the BLA (number in top left corner depicts distance from bregma) and adjacent eYFP-positive terminals in the CeL (scale bar 150μm); location of terminals was independently verified and repeated in n=2 mice. **b,** Experimental paradigm for dual patch-clamp recordings from neighboring CRF+ and CRF− neurons in fear conditioned and fear extinguished mice. Bottom-right: DIC and fluorescent overlay image of dual-patch clamp recording from CRF+ and CRF− pair. **c,** Traces of maximal oEPSC amplitude from CRF+ (red) and CRF− (black) neuronal pairs across behavioral conditions for stimulation of the BLA-CeL circuit (scale bars 10ms, 100pA for basal, and 10ms, 400pA for fear and extinction). **d,** XY graphs depicting skew-plot of maximal oEPSC amplitude from each CRF + and CRF− neuronal pair for behavioral conditions (n=19 basal pairs, 5 mice, n=18 fear pairs, 5 mice, and n=18 extinction pairs, 5 mice; extra sum-of-squares F test, $F_{(1,18)}$=92.68, P<0.0001 for basal, and $F_{(1,17)}$=45.08, P=0.0001 for extinction). **e,** Representation of CRF +/CRF− maximal oEPSC amplitude ratio (log scale; n=19 basal pairs, n=18 fear pairs, and n=18 extinction pairs; Kruskal-Wallis test, P=0.0021; post-hoc Dunn's multiple comparisons, basal vs. fear P=0.0011, fear vs. extinction P=0.0442). XY skew-plots are presented as absolute value. Bar graphs are presented as mean + S.E.M. *P<0.05, **P<0.01, ***P<0.001, ****P<0.0001.

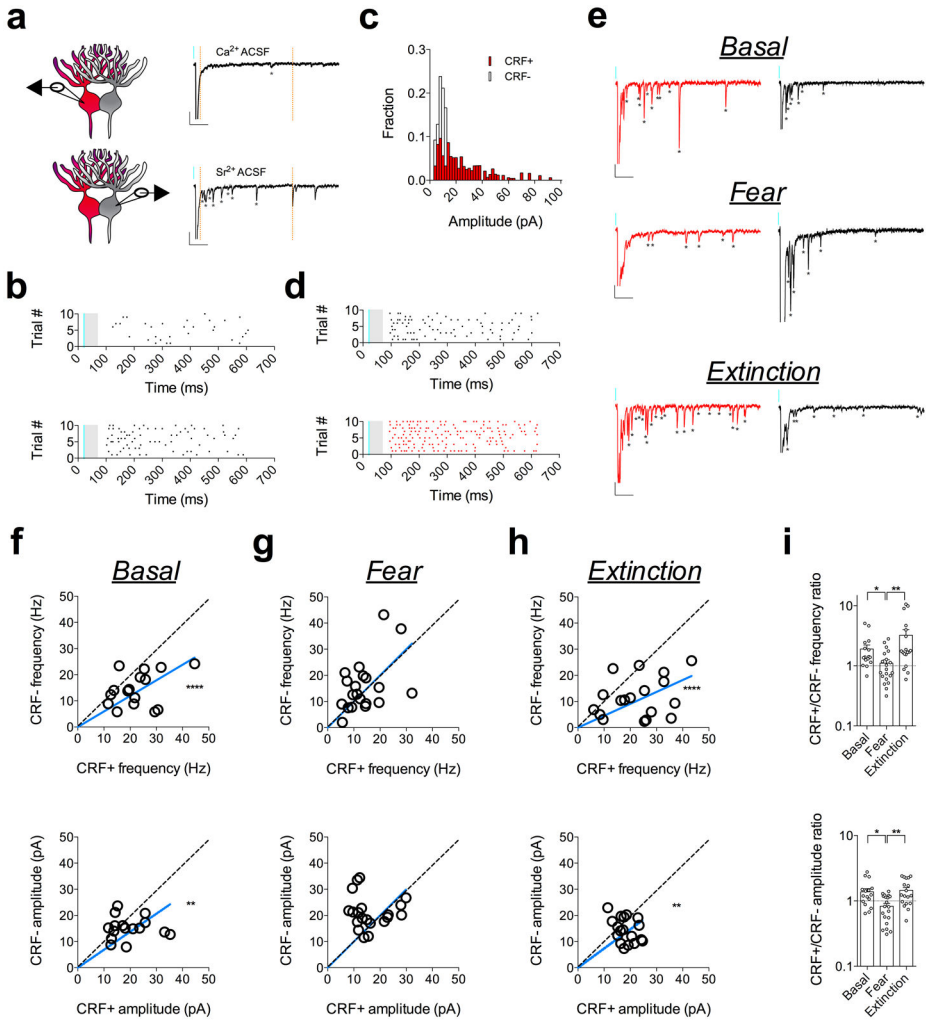

Fig. 4. Experience-dependent remodeling of BLA-CeL input bias is driven by presynaptic and postsynaptic alterations.

a, Alternating patch-clamp technique with representative traces from a CeL-cell recorded in the presence of extracellular calcium or strontium (scale bars 100ms, 20pA). **b,** Raster plot of asynchronous events in the presence of extracellular calcium or strontium for the cell depicted in panel a. **c,** Example of amplitude distribution from a recording of neighboring CRF+ and CRF− neurons. **d,** Raster plot of asynchronous events from example in panel c. **e,** Representative traces of strontium induced asynchronous release from neighboring CRF+ and CRF− neurons across fear states (*indicates presence of asynchronous event, scale bars 100ms, 20pA). **f,** XY graphs depicting skew-plot of aEPSC frequency (top) and amplitude (bottom) for neighboring CRF+ and CRF− neurons in naïve mice (basal condition) (n=16 pseudopairs, 4 mice; extra sum-of-squares F test, $F_{(1,15)}$=33.96, P<0.0001 for aEPSC frequency, and $F_{(1,15)}$=14.48, P=0.0017 for aEPSC amplitude). **g,** XY graphs depicting skew-plot of aEPSC frequency and amplitude for neighboring CRF+ and CRF− neurons in fear conditioned mice (n=20 pseudopairs, 4 mice). **h,** XY graphs depicting skew-plot of aEPSC frequency and amplitude for neighboring CRF+ and CRF− neurons after fear extinction training (n=18 pseudopairs, 4 mice; extra sum-of-squares F test, $F_{(1,17)}$=54.07,

$P<0.0001$ for aEPSC frequency, and $F_{(1,17)}=11.02$, $P=0.0041$ for aEPSC amplitude) **i,** Representation of CRF+/CRF− frequency and amplitude ratios from neighboring CRF+ and CRF− neurons during aEPSC recordings (log scale; $n=16$ basal pseudopairs, $n=20$ fear pseudopairs, $n=18$ extinction pseudopairs for each group; Kruskal-Wallis tests, $P=0.0035$ for frequency and $P=0.0030$ for amplitude; post-hoc Dunn's multiple comparisons, basal vs. fear frequency $P=0.0405$, fear vs. extinction frequency $P=0.0025$, basal vs. fear amplitude $P=0.0112$, fear vs. extinction amplitude $P=0.0049$). XY skew-plots are presented as absolute value. Bars graphs are presented as mean + S.E.M. *$P<0.05$, **$P<0.01$, ****$P<0.0001$.

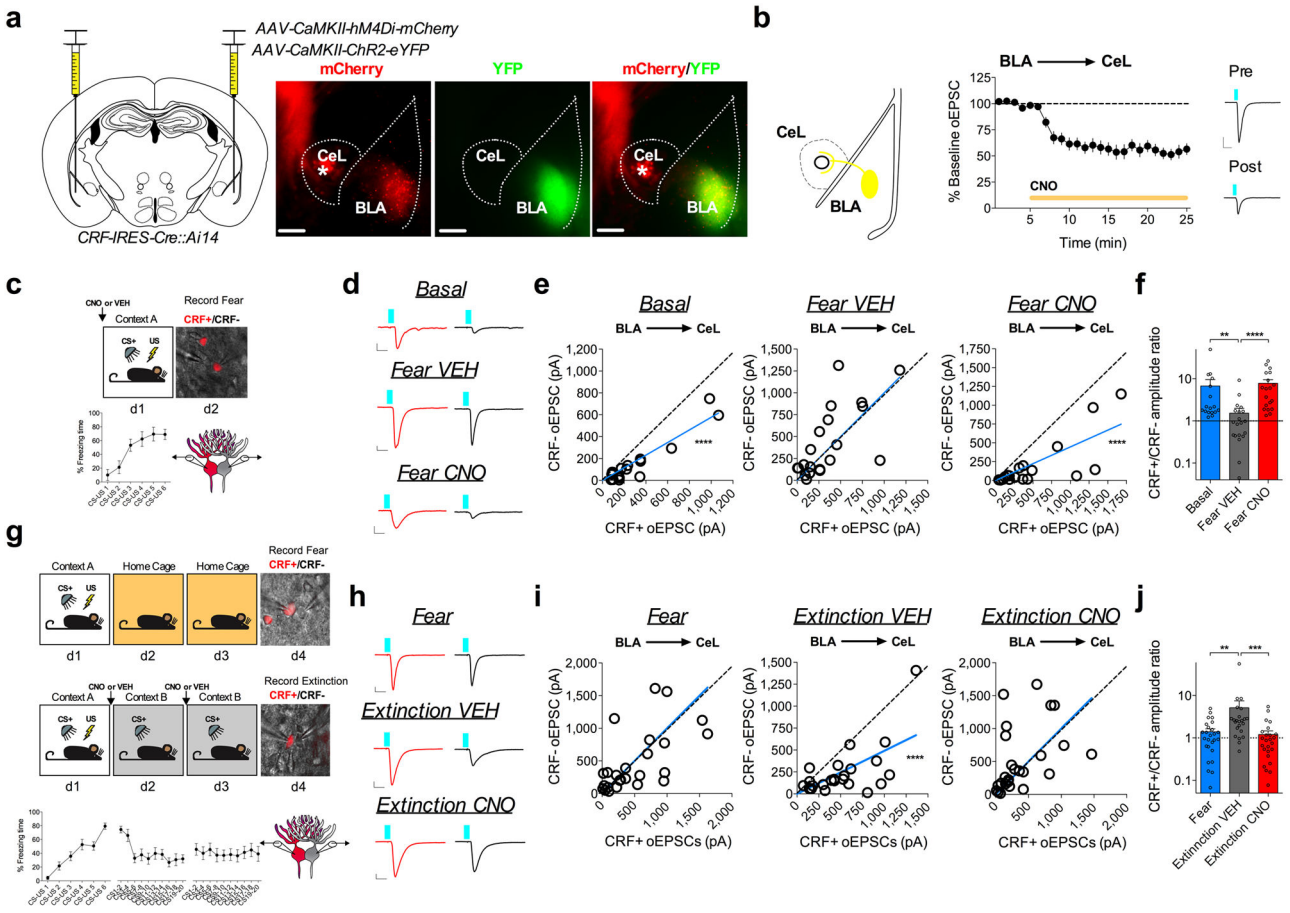

Figure 5. BLA activity is necessary for remodeling input bias onto CRF+ and CRF− neurons.

a, Left: mixed viral injection strategy for electrophysiological assessment of inhibiting the BLA-CeL circuit. Right: image of ChR2-eYFP and hM4D(Gi)-mCherry expression in the BLA from a coronal slice used for recordings (*indicates CRF+ neurons in the CeL expressing TdTomato; scale bars 200μm); viral expression strategy was independently verified in n=4 mice. **b,** Top-left: depiction of co-infected ChR2-eYFP and hM4D(Gi)-mCherry projection of the BLA-CeL. Middle: Summary data from bath application of CNO while recording oEPSC amplitude in the CeL (see methods; n=13 cells, 5 mice). Right: traces of oEPSCs before and after bath application of CNO (scale bar 10ms, and 200pA). **c,** Left: experimental paradigm of electrophysiological assessment of inhibiting the BLA prior to fear conditioning. Right: DIC and fluorescent overlay image of dual-patch clamp recording from CRF+ and CRF− pair. Bottom: fear learning curve from 10 mice used for recordings. **d,** Traces of maximal oEPSC amplitude from CRF+ (red) and CRF− (black) neuronal pairs across treatment groups (scale bars 10ms, and 50pA). **e,** XY graphs depicting skew-plot of maximal oEPSC amplitude from each CRF+ and CRF− neuronal pair across conditions (n=17 basal pairs, 5 mice, n=20 fear VEH pairs, 5 mice, and n=19 fear CNO pairs, 5 mice; extra sum-of-squares F test, $F_{(1,16)}$=105.5, P<0.0001 for basal, $F_{(1,18)}$=65.60, P=0.0002 for fear CNO). **f,** Representation of CRF+/CRF− maximal oEPSC amplitude ratio (log scale; n=17 basal pairs, n=20 fear VEH pairs, and n=19 fear CNO pairs; Kruskal-Wallis test, P<0.0001; post-hoc Dunn's multiple comparisons, basal vs. fear VEH P=0.0048, fear

VEH vs. fear CNO $P<0.0001$). **g,** Top: experimental paradigm for BLA inhibition prior to fear extinction training sessions and time-matched fear controls. Bottom: fear learning curve from 15 mice, and extinction learning curves from 10 mice used for recordings. **h,** Traces of maximal oEPSC amplitude from CRF+ (red) and CRF− (black) neuronal pairs across treatment groups (scale bars 10ms, and 100pA). **i,** XY graphs depicting skew-plot of maximal oEPSC amplitude from each CRF+ and CRF− neuronal pair across conditions ($n=26$ fear pairs, 4 mice, $n=23$ extinction VEH pairs, 5 mice, and $n=25$ extinction CNO pairs, 5 mice; extra sum-of-squares F test, $F_{(1,22)}=46.26$, $P<0.0001$). **j,** Representation of CRF+/CRF− maximal oEPSC amplitude ratio (log scale; $n=26$ fear pairs, $n=23$ extinction VEH pairs, and $n=25$ extinction CNO pairs; Kruskal-Wallis test, $P=0.0002$; post-hoc Dunn's multiple comparisons, fear vs. extinction VEH $P=0.0035$, extinction VEH vs. extinction CNO $P=0.0002$). XY skew-plots are presented as absolute value with lines through origin. Time-points for CNO bath application and learning curves for behavioral experiments are depicted as mean ± S.E.M. Bar graphs are presented as mean + S.E.M. *$P<0.05$, **$P<0.01$, ***$P<0.001$, ****$P<0.0001$.

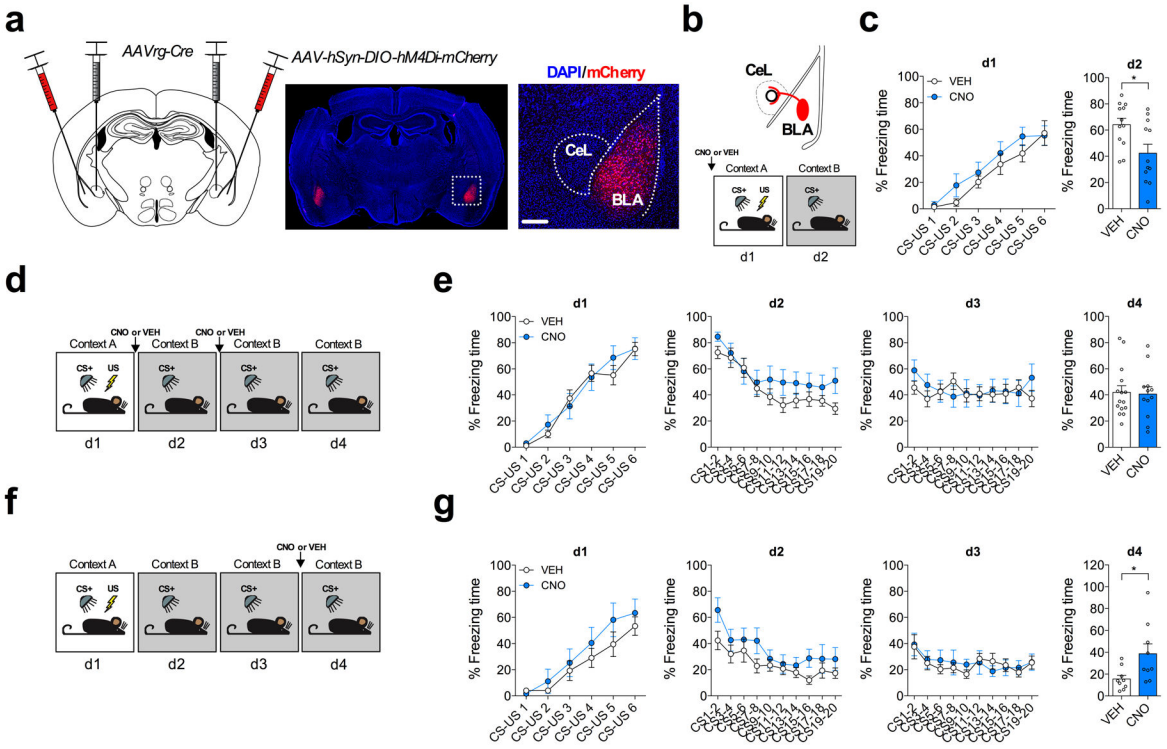

Fig. 6. BLA-CeL circuit activity is required for optimal fear memory acquisition and the retrieval of extinction memory.

a, Left: intersectional viral strategy for BLA-CeL circuit inhibition. Right: images depicting bilateral expression of cre-dependent hM4D(Gi)-mCherry in the BLA with close up of inset (scale bar 200μm); viral expression strategy was independently verified in n=14 mice. **b,** Top: schematic of hM4D(Gi)-mCherry expression specifically in BLA neurons projecting to the CeL. Bottom: experimental paradigm for behavioral assessment of BLA-CeL circuit inhibition during fear conditioning. **c,** Learning curve for VEH or CNO-treated mice during fear acquisition on day 1 (d1), and fear memory recall on day 2 (d2) drug-free (n=12 mice per group; two-tailed unpaired t-test, $t_{(22)}$=2.576, P=0.0172). **d,** Experimental paradigm for behavioral assessment BLA-CeL circuit inhibition during extinction training. **e,** Learning curves for VEH and CNO-treated mice. Left to right, conditioning day 1 (d1), extinction sessions 1-2 (d2-d3), and extinction memory recall test on day 4 (d4) (n=15 mice for VEH, and n=12 mice for CNO). **f,** Experimental paradigm for behavioral assessment of BLA-CeL circuit inhibition during an extinction memory recall test. **g,** Learning curves for VEH and CNO treated mice. Left to right, conditioning day 1 (d1), extinction sessions 1-2 (d2-d3), and extinction memory recall test on day 4 (d4) (n=9 mice per group; two-tailed unpaired t-test, $t_{(16)}$=2.394, P=0.0293). Learning curves are presented as mean ± S.E.M. and bar graphs are presented as mean + S.E.M. *P<0.05.

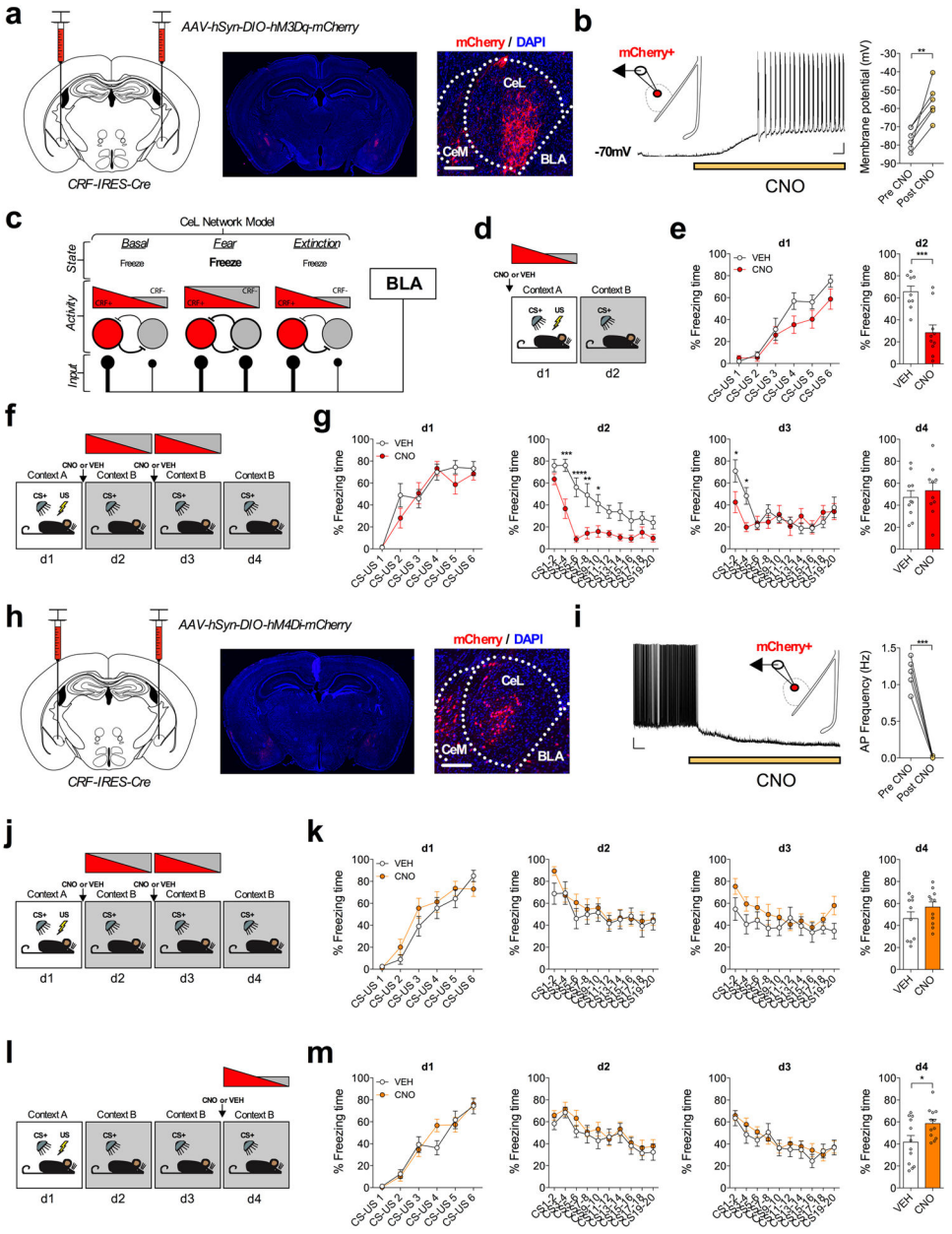

Fig. 7. CRF+ neuron activity impairs fear memory acquisition, facilitates within session extinction, and is necessary for extinction retrieval.

a, Left: injection strategy for cre-dependent hM3D(Gq)-mCherry expression in CRF+ neurons of the CeA. Right: images depicting bilateral targeting of hM3D(Gq)-mCherry to CRF neurons in the CeA with magnification demonstrating mCherry fluorescence (scale bar 200μm); viral expression was independently verified in n=3 mice. **b,** Patch-clamp recording from mCherry+ neurons in the CeL with representative trace of CNO bath application causing depolarization to action potential threshold in mCherry+ neuron (scale bar 0.5min, and 10mV). Right: Summary of change in resting membrane potential following bath application of CNO (n=6 cells, 3 mice; two-tailed paired t-test, $t_{(5)}$=4.864, P=0.0046). **c,** Proposed model for the BLA-CeL circuit remodeling across fear states. **d,** Experimental

paradigm for enhancing excitability of CeA-CRF+ neurons during fear conditioning with input bias depicted at time of injection. **e,** Learning curves for VEH and CNO-treated mice. Left to right, conditioning day 1 (d1), fear memory recall test on day 2 (d2) (n=9 VEH mice, and n=10 CNO mice; two-tailed unpaired t-test, $t_{(17)}$=4.202, P=0.0006). **f,** Experimental paradigm for enhancing excitability of CeA-CRF+ neurons during extinction training with activity bias depicted at time of injection. **g,** Learning curves for VEH and CNO-treated mice. Left to right, conditioning day 1 (d1), extinction session 1-2 (d2-d3), and extinction memory recall test on day 4 (d4) (n=10 mice per group; two-way repeated measures ANOVA, $F_{(1,18)}$=20.19, P=0.0003 for effect of treatment; post-hoc Holm-Sidak's multiple comparisons, d1 CS3-4 P=0.0001, CS5-6 P<0.0001, CS7-8 P=0.0011, CS9-10 P=0.0335, d2 CS1-2 P=0.0272, CS3-4 P=0.0272). **h,** Left: injection strategy for cre-dependent hM4D(Gi)-mCherry expression in CRF+ neurons of the CeA. Right: images depicting bilateral targeting of hM4D(Gi)-mCherry to CRF neurons in the CeA with magnification demonstrating mCherry fluorescence (scale bar 200μm); viral expression strategy was independently verified in n=2 mice. **i,** Patch-clamp recording from mCherry+ neurons in the CeL with representative trace of CNO bath application causing hyperpolarization and reduction in action potential frequency (scale bar 0.5min, and 10mV). Right: Summary of change in action potential frequency following bath application of CNO (n=5 cells, 3 mice, two-tailed paired t-test, $t_{(4)}$=12.23, P=0.0003). **j,** Experimental paradigm for decreasing excitability of CeA-CRF+ neurons during extinction training with input bias depicted at time of injection. **k,** Learning curves for VEH and CNO-treated mice. Left to right, conditioning day 1 (d1), extinction sessions 1-2 (d2-d3), and extinction memory recall test on day 4 (d4) (n=10 VEH mice, and n=11 CNO mice). **l,** Experimental paradigm for decreasing excitability of CeA-CRF+ neurons during an extinction memory recall test with input bias depicted at time of injection. **m,** Learning curves for VEH and CNO-treated mice. Left to right, conditioning day 1 (d1), extinction sessions 1-2 (d2-3), and extinction memory recall test on day 4 (d4) (n=12 mice per group; two-tailed unpaired t-test, $t_{(22)}$=2.334, P=0.0291). Learning curves are presented as mean ± S.E.M., and bar graphs are presented as mean + S.E.M. *P<0.05, **P<0.01, ***P<0.001, ****P<0.0001.